A Numerical Simulation of the Variability in the Tropical Atlantic Ocean, 1980–88

BOHUA HUANG, JAMES A. CARTON, AND J. SHUKLA

Center for Ocean–Land–Atmosphere Studies, Institute of Global Environment and Society, Calverton, Maryland

(Manuscript received 8 November 1993, in final form 25 July 1994)

ABSTRACT

The authors have examined a numerical simulation of the tropical Atlantic Ocean circulation forced by the European Centre for Medium-Range Weather Forecasts (ECMWF) surface wind stress during 1980–88. The mean state and annual cycle of the ocean are realistically simulated by the model. The simulated interannual variability of sea surface temperature (SST) is also remarkably consistent with the observations, particularly the observed patterns of the basinwide warm/cold periods and the variation of dipole pattern and the associated meridional SST gradient. Discrepancies between observed and simulated SST anomalies are large early in the simulation, which seems caused by errors in the ECMWF wind analysis during that period.

The low-frequency fluctuations of the meridional SST gradient associated with the dipole pattern during 1980–88 were caused by opposite SST anomalies between hemispheres, forced by out of phase fluctuations of the trade winds. Specifically, the southeast trade winds were anomalously strong during 1981–83 and weaker than normal during 1985–86 and 1987–88. The northeast trade winds, on the other hand, showed nearly opposite variation, being weak in 1980–83 and strong in 1985–86. In the northern ocean, SST was higher during 1980–83 but lower during 1985–86 as the local trade winds were weak and strong. On the other hand, as the southeast trades and the equatorial easterlies were strong in 1981–83, the slope of the thermocline was anomalously steep along the equator and both the South Equatorial Current and the Equatorial Undercurrent intensified. Forced by the anomalous equatorial easterlies, warm water diverged from the equator into the Tropics in the western ocean. In the southeastern portion of the basin, the thermocline was shallow and SST was anomalously low. When the southeast trade winds were weakened in 1984, warm water converged toward the equator from both hemispheres, and then shifted into the southeast part of the ocean. The heat anomalies were maintained there during 1985/86, when the southeast trades were weak, deepening the thermocline and causing anomalously high SST. Therefore, unlike those in the northern Tropics, SST fluctuations in the southeastern part of the ocean are related to the basinwide adjustment of the ocean and net heat transport across the equator in response to the equatorial wind anomalies.

1. Introduction

The variability in the tropical Atlantic Ocean is dominated by a strong annual cycle forced by the surface wind stress. Superimposed on the annual cycle are fluctuations on interannual and decadal timescales, which, though weaker than the annual change, show systematic variations and are considered to be one of the most important factors causing regional climate anomalies, such as drought conditions in sub-Sahara, Northeast Brazil, and the Angola coast (e.g., see Lamb 1978a, b; Markham and Mclain 1977; Hastenrath and Heller 1977; Moura and Shukla, 1981; Hirst and Hastenrath 1983; Nobre 1993; Nobre and Shukla 1995). Although the annual cycle in the tropical Atlantic Ocean has been intensively investigated through observations, modeling, and theoretical studies (see reviews by Cane and Houghton 1987; Busalacchi 1987; Cane and Busalacchi 1987), our knowledge of the mechanism of interannual changes is limited.

Corresponding author address: Dr. Bohua Huang, COLA/IGES, 4041 Powder Mill Road, Suite 302, Calverton, MD 20705-3106.

Due to the limitation of data coverage, the interannual fluctuations in the tropical ocean are mainly detected from the sea surface temperatures (SSTs). Empirical orthogonal function (EOF) analyses of Atlantic SST measurements show two dominant interannual modes (see, e.g., Servain 1991). One mode represents a basinwide oscillation of two to three years, which is mainly composed of warm and cold events centered in the equatorial ocean (Philander 1986; Zebiak 1993; Carton and Huang 1994). These equatorial SST fluctuations may be associated with air–sea interactions within the tropical Atlantic region (Zebiak 1993) or atmospheric disturbances in the tropical Atlantic sector caused by the El Niño–Southern Oscillation (ENSO) (Horel et al. 1986). The other mode has considerable variability on decadal timescales and has its largest fluctuations in the subtropics. Its spatial structure is characterized by a dipole straddling the thermal equator (Weare 1977; Moura and Shukla 1981; Servain and Legler 1986; Lough 1986; Servain 1991; Servain and Merle 1993). The decadal variability of the dipole pattern has been found to be linked to anom-

alous rainfall in the sub-Sahara and northeast Brazil.

It should be noted that the notion of characterizing the decadal SST variability as a coherent dipole oscillation has been questioned. In EOF analyses of the SST anomalies, the dipole structure is usually derived as the second leading mode. Houghton and Tourre (1992) have argued that this structure is forced by the constraint of spatial orthogonality in EOF analysis. Using EOF modes rotated by varimax method and simple correlations of area-averaged temperatures, they claimed that SST anomalies to the south and north of the intertropical convergence zone (ITCZ) are not significantly correlated. On the other hand, Nobre and Shukla (1994) demonstrated that the SST dipole does appear as the first mode in a combined EOF analysis of SST and surface wind stress, which is not only free from the restriction of spatial orthogonality but is also physically consistent with a pattern of the surface wind. The low correlation between SSTs in the south and north may also be due to destructive interference between changes in the dipole pattern and other fluctuations such as the basinwide warm–cold mode. In fact, both points of view support the fact that there is decadal fluctuation of the meridional SST gradient near the equator. By analyzing data alone it is not possible to determine whether the fluctuations are due to coherent but out of phase changes between hemispheres or whether they represent two independent variations. A persuasive answer requires further understanding of dynamics in both the atmosphere and the ocean.

During the 1980s, the tropical Atlantic SST experienced anomalous warm events during 1984 and 1987–88 in the Gulf of Guinea, with the former event having the strongest intensity since 1963 (Philander 1986; Carton and Huang 1994). The meridional SST gradient across the equator also experienced major changes during this period. From the mid-1970s, the SST was maintained higher than its long-term climatology in the northern ocean, but lower in the southern ocean, forming a northward anomalous temperature gradient in the equatorial ocean. Following the warm event in 1984, the temperature increased to the south of the equator rapidly (Lamb et al. 1986), so that the anomalous meridional temperature gradient reversed to southward. This southward gradient changed sign temporarily in early 1987 but strengthened again in 1988, following another warm event (Servain 1991). The drastic change of the north–south temperature gradient in the mid-1980s provides an opportunity to examine its possible mechanisms.

We have analyzed a numerical simulation of the tropical Atlantic Ocean by an ocean general circulation model forced with observed monthly mean surface wind stress for 1980–88. The main questions addressed are the following: Can the ocean model simulate the interannual variability of the SST in the tropical Atlantic Ocean during 1980–88, especially the fluctuation of the SST gradient near the equator and how is the oceanic interannual variability related to the ocean dynamics and the surface wind forcing? We find that the fluctuations of the meridional SST gradient in the 1980s are realistically reproduced by the model, which is associated with low-frequency antisymmetric SST signals between hemispheres caused by an out of phase interannual change between the northeast and the southeast trade winds. Moreover, the SST anomalies in the eastern tropical South Atlantic are closely related to the heat content anomalies originated in the western ocean both to the north and south of the equator, which moves first eastward and then into the Southern Ocean in response to equatorial wind changes.

In the next section, the experiment is described. The simulated variation of the SST and its relationship to variations in surface wind are discussed in section 3. The changes in the ocean thermocline and circulation are discussed in sections 4 and 5. Finally, a summary is given in section 6.

2. The experiment

The Geophysical Fluid Dynamics Laboratory (GFDL) ocean general circulation model (Philander and Pacanowski 1986a) was used for the simulation. The model solves the system of primitive equations with the hydrostatic and Bousinesq approximations. Its domain includes the Atlantic Ocean from 30°S to 50°N with zonal resolution of 1° throughout the basin and meridional resolution 1/3° equatorward of 10° and gradually coarser toward higher latitudes. It has 27 levels in the vertical, with a constant interval of 10 m for the upper 100 m. Its basin geometry and topography are realistic with a no-slip condition imposed at the coast as well as the artificial north and south boundary at 30°S and 50°N. To minimize the effects of the artificial walls at southern and northern boundaries, oceanic temperature and salinity at higher latitudes are relaxed to observed monthly climatology. Horizontal mixing and diffusion are calculated with a constant coefficient of 2×10^7 cm^2 s^{-1}. The coefficients for vertical mixing and diffusion are Richardson number–dependent following Pacanowski and Philander (1981).

The model is forced with surface wind stress and heat flux. The surface heat flux is composed of radiative, sensible, and evaporative heat fluxes. For this simulation, heating due to incident solar radiation is assumed to be a constant, representing its annual climatology within 10°S and 10°N and decreasing linearly to the north and south. The longwave radiation is constant over the whole basin. Sensible and latent heating are calculated from bulk formula depending on the difference between specified climatological monthly air temperature and model-predicted SST, as well as surface wind speed.

In the model, the latent and sensible heat fluxes damp SST departure from a prescribed annual cycle

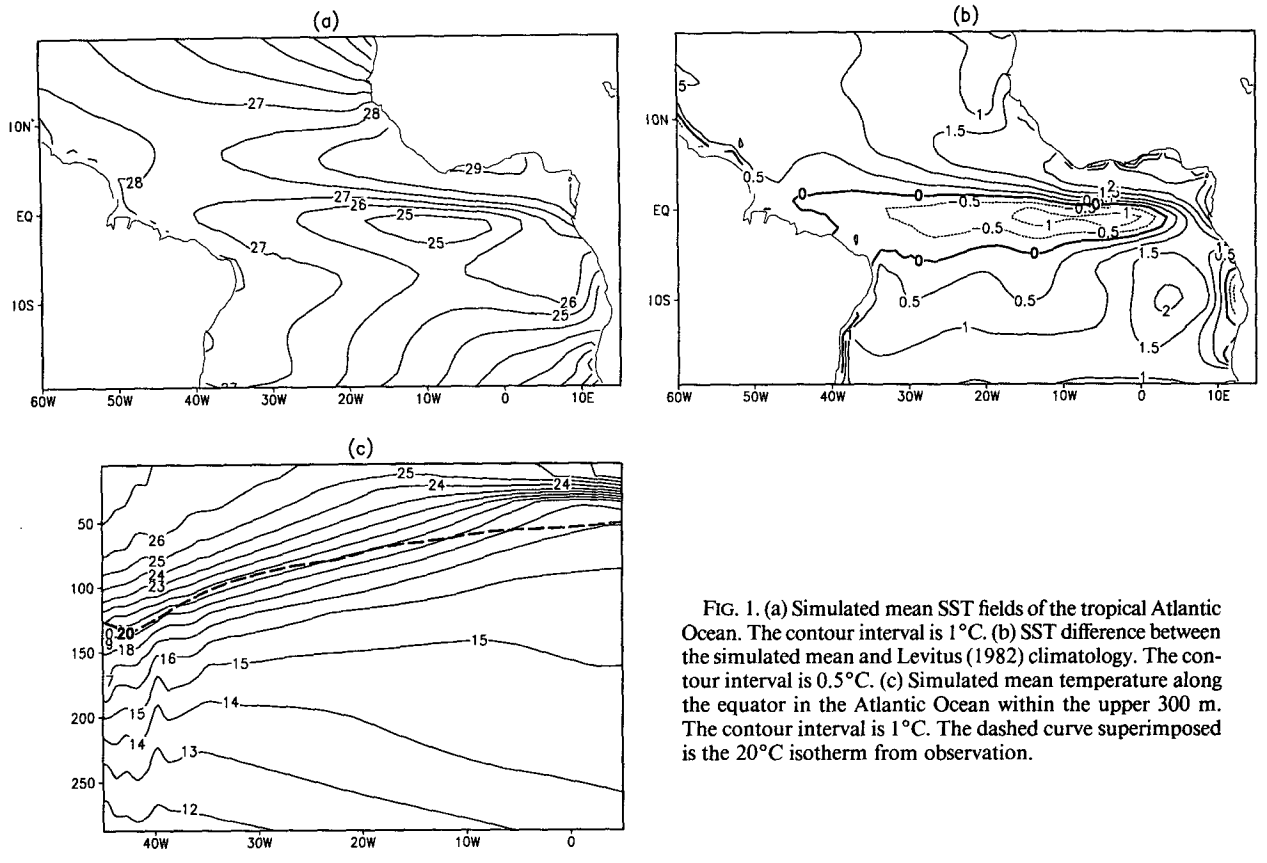

FIG. 1. (a) Simulated mean SST fields of the tropical Atlantic Ocean. The contour interval is 1°C. (b) SST difference between the simulated mean and Levitus (1982) climatology. The contour interval is 0.5°C. (c) Simulated mean temperature along the equator in the Atlantic Ocean within the upper 300 m. The contour interval is 1°C. The dashed curve superimposed is the 20°C isotherm from observation.

of the climatological air temperature. In reality, the air temperature itself changes interannually. However, in a heat flux formulation based on prescribed surface air temperature and model SST, a prescribed interannual signal of the surface air temperature may induce similar SST signals directly and locally, even without wind change. This may obscure the important effects of wind forcing and ocean dynamics in the generation of the SST anomalies. On the other hand, given an SST change caused by wind forcing/ocean dynamics, air temperature usually follows the SST change, and the sensible and evaporative heat fluxes at the sea surface tend to damp the SST anomaly. The climatological air temperature is used because it represents this process reasonably.

The surface wind stress is calculated from twice-daily European Centre for Medium-Range Weather Forecasts (ECMWF) 1000-mb wind by bulk aerodynamical formula using surface air density ρ and a drag coefficient C_D. In turn, C_D is derived from wind speed and monthly climatology of COADS (Comprehensive Ocean–Atmosphere Data Set) SST, relative humidity, and sea–air temperature difference based on the Trenberth et al. (1990) formulation. Surface air density ρ is also inferred from ECMWF data. The stress is computed at a spatial resolution 2.5° × 2° and monthly averaged. The characteristics of the wind field data have been described in detail by Huang and Shukla (1995).

The initial conditions correspond to an ocean at rest with climatological temperature and salinity in January (Levitus 1982). The model is first spun up for six years forced by the ECMWF nine-year mean monthly climatology to obtain quasi-equilibrium ocean conditions. Thereafter, the wind stress for each month for the period of 1980–88 is used for a nine-year simulation of the ocean circulation.

3. Sea surface temperature

a. Mean state and annual cycle

The simulated nine-year mean SST field of the tropical Atlantic Ocean (Fig. 1a) shows a zonal belt of high temperature north of the equator, spanning about 10° of latitude in the mean position of the ITCZ. In this belt, the warmest water is located in the west (SST > 28°C) and in the Gulf of Guinea (SST near 30°C). Outside this belt, temperature generally decreases with increasing latitude in both hemispheres. Low temperatures also appear in the equatorial central and eastern

ocean and near the subtropical African coast due to the equatorial and coastal upwelling.

These broad features of the simulated SST fields are consistent with the observations over the tropical Atlantic Ocean. However, significant quantitative differences from the observations also exist. The simulated SST is about 1°C colder than observed around the equator (Fig. 1b) due to errors in the depth of the thermocline in the eastern ocean (Fig. 1c). Another major error in the simulated SST is that temperature near the northern coast of the Gulf of Guinea is more than 1°C warmer than observed. Off the equatorial ocean, the simulated temperatures also tend to be warmer, but are generally within 2°C of the observed values. These discrepancies seem to reflect a systematic bias of present OGCMs in the Tropics for both Atlantic and Pacific Oceans (Chao and Philander 1993).

The annual cycle of the simulated SST off the equator is dominated by an oscillation between the hemispheres with sea surface warmer in the summer–autumn hemisphere (Figs. 2a,b), qualitatively similar to the observation (Figs. 2c,d). This change is due to the seasonal variations of the prescribed wind forcing and surface air temperature. The trade wind change induces stronger coastal upwelling in the winter and spring, which causes SST fluctuations of 3°C in the east. The changes of air temperature modulates sensible and latent heat fluxes into the ocean and may contribute toward the annual migration of warm water. Near the equator, SST changes in the eastern ocean are related to the annual fluctuations of the zonal slope of the equatorial thermocline caused by the changes in equatorial easterly winds. The cold tongue is weak in late boreal winter and spring and strengthened in May–June. Overall, the simulated and observed seasonal cycles of the SST fields have similar patterns and comparable annual amplitudes.

b. Interannual variability

We examine how well the major interannual modes of the tropical Atlantic Ocean SST fluctuations are re-

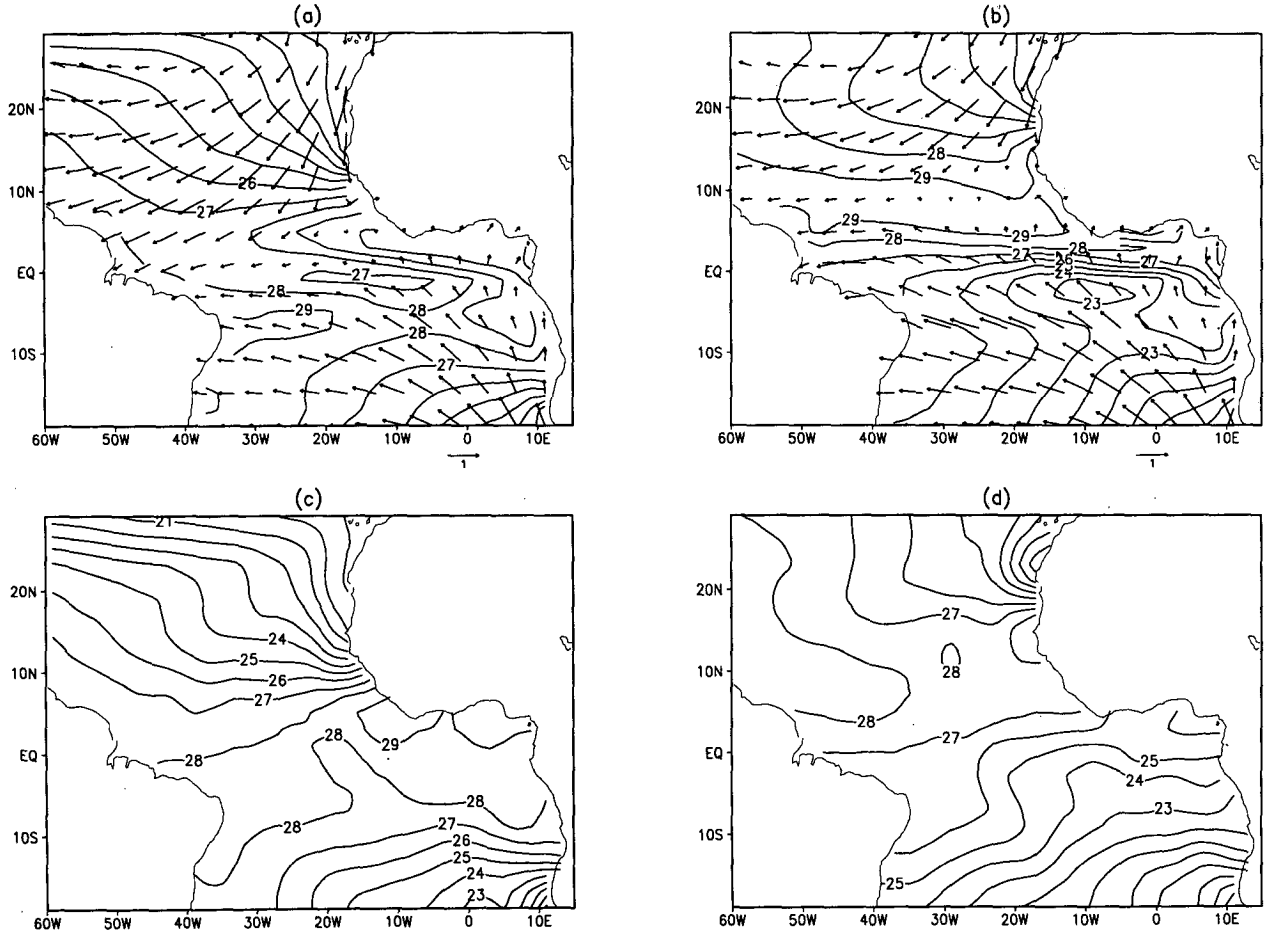

FIG. 2. Monthly climatological mean SST from the model for (a) April and (b) September, with corresponding monthly climatological surface wind stress forcings and monthly climatological mean SST from observations (Servain et al. 1987) for (c) April and (d) September. The contour interval is 1°C for SST and the unit of wind stress is dynes per square centimeter.

produced by the model. The interannual signals are investigated by examining SST anomalies with respect to an annual cycle. Four indices (Servain 1991) are used to measure the interannual variations. The TB index is defined as SST anomaly averaged between 20°S and 30°N and normalized by its standard deviation for each month. Similarly, the NB and SB indices are defined as SST anomalies respectively averaged within 5°–30°N and 20°S–5°N. The dipole index is defined as the difference of the NB and SB indices.

Apparently, the TB index describes the SST fluctuations over the whole basin. The dipole index is defined to quantify the fluctuations of the dipole pattern between the Northern and Southern Hemispheres (Servain 1991). Here we use it to represent the meridional SST gradient near the equator and refer to it as DP index later on. Actually, these two indices allow a balanced view of the two SST anomaly patterns revealed by conventional EOF analysis, the basinwide warm/cold mode and the meridional dipole. On the other hand, Houghton and Tourre (1992) showed that indices defined similar to NB and SB to represent the SST variability in the north and south are good indicators of the temporal feature of the two leading rotated EOF modes of the tropical Atlantic SST anomalies.

Figure 3 shows these four indices calculated from the simulated monthly SST anomalies for the period of 1980–88 (the solid curves) and the corresponding observed indices for a longer period represented by the dashed curves. The observed NB and SB indices (Figs. 3a,b, dashed curves) show oscillations on decadal timescales. The NB indices from observation and simulation (Fig. 3a) both decreased in 1980–86 and increased in 1987–88, with a stronger increase in observations. The observed and simulated SB indices (Fig. 3b) generally increased during 1982–88 except for a temporary setback in 1986.

The observed DP index (Fig. 3c, dashed line) also shows decadal fluctuations. In the 1980s, a major change in the observed DP index occurred, implying that SST changed from a pattern of northward gradient prevailing since the mid-1970s to its opposite in 1983–84, which then persisted to the end of the period examined here, though with a temporary break in 1987. Due to the relatively short length of the simulation, the nature of decadal fluctuations of the dipole cannot be resolved by the simulated DP index. However, by comparing the two curves in Fig. 3c in their common period, we can see that the model did very well in simulating the DP fluctuations during 1980–88. On the other hand, both the simulated and the observed TB indices (Fig. 3d) are dominated by fluctuations with timescales of several years and have similar behavior during 1983–88. Specifically, the model reproduced the observed basinwide cold periods in 1986 and warm periods in 1984 and 1987–88.

Although there are strong low-frequency fluctuations of the DP index, the correlation between the simulated NB and SB is weak (0.14). This number is close to the observed value (0.23) given by Servain (1991) based on the monthly SST anomalies for 1964–90. Therefore, NB and SB tend to fluctuate independently in both the observation and the model if variations on all scales are considered. However, this does not exclude the possibility that the variations picked up by the DP index on decadal timescales represent coherent oscillation between the north and the south, because both NB and SB are also affected by other modes such as the basinwide warming/cooling, and their destructive interference with the dipole fluctuation may reduce the correlation between NB and SB significantly.

Noticeable discrepancy between the simulated and observed indices appears in the early 1980s (Fig. 3). For example, the simulated SB and TB indices show warming in 1980 followed by a strong cooling in 1981, a change not seen in the observations. The largest error of the simulated DP index also occurred before 1982. Since the wind forcing switched from the climatological monthly means to the actually observed fields in January 1980, it may cause model adjustment in this period. On the other hand, the error may also be related to the poor quality of the wind data in the early 1980s when frequent changes of the ECMWF analysis/forecast system might induce artificial signals. Huang and Shukla (1994) have examined the difference between the ECMWF surface wind stress and another surface wind stress dataset independently constructed from ship observations over the tropical Atlantic Ocean (Servain 1987) and their effects on OGCM simulations during 1980–87. It was found that the southeast trades were weak in 1980 in the ECMWF wind stress data, followed by a large increase in 1981. This pattern was not detected in the other dataset. Actually, when the latter wind was used to replace the ECMWF winds in the Tropics in forcing the ocean model, better agreement between the model and the observation was found in these two years (Huang and Shukla 1994).

The relationship between the wind stress and the simulated SST anomalies is also investigated. Figure 4 shows the NB, SB, DP, and TB indices of the zonal wind stress anomalies (the dash curves) together with the corresponding SST indices (the solid curves) during 1980–88. Most remarkable are the in-phase variations of the corresponding indices, with highest correlation between the DP indices of the SST and the zonal wind stress (0.85). The NB and SB indices of the meridional wind stress anomalies (not shown) are also significantly correlated with the corresponding SST indices (0.63 for NB and −0.48 for SB), but their DP and TB indices are nearly uncorrelated between the meridional winds and SSTs (−0.2 for DP and 0.2 for TB).

We have also examined the leading modes of a singular value decomposition (SVD) analysis between SST and wind stress anomalies. The SVD technique allows for an analysis of the linear correlation of two fields (e.g., see Prohaska 1976; Lanzante 1984; Breth-

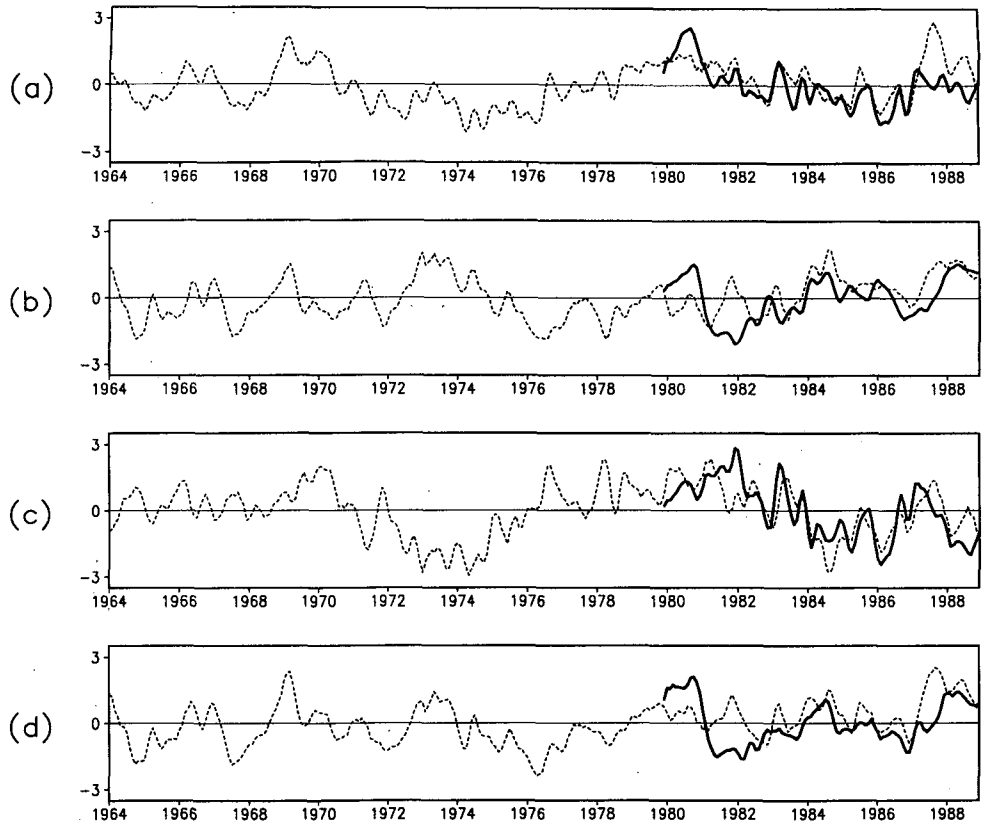

FIG. 3. Observed (dash line) and simulated (solid line) indices characterizing the dominant modes of the interannual SST variability in the tropical Atlantic Ocean for the (a) NB index, (b) SB index, (c) DP index, and (d) TB index.

erton et al. 1992; Wallace et al. 1992). Applied to a covariance matrix of two datasets, the SVD identifies pairs of spatial patterns that explain the maximum possible mean squared temporal covariance. These patterns are referred to as SVD patterns. The temporal fluctuations of the SVD patterns are determined by the SVD time series that are the projections of the data fields onto the corresponding patterns. The SVD patterns and the time series together form an SVD mode. In practice, an SVD pattern is usually scaled such that the value at each grid point is equivalent to the temporal correlation coefficient between the SVD time series and the field variable at the same grid point, which will be referred to as heterogeneous correlation maps here, following Bretherton et al. (1992). The SVD analysis is performed for the temporarily normalized surface wind stress and SST anomalies in the tropical Atlantic Ocean to the east of 60°W and within 20°S–30°N, with both wind components combined as one variable.

Figure 5 shows the first SVD mode of the SST and wind stress anomalies, which explains 23% of the covariance as well as 18% of the normalized ECMWF wind stress and 23% of the simulated SST anomalies. The heterogeneous map (Fig. 5a) shows a pattern of northeast wind anomalies over the tropical Atlantic Ocean to the north of 10°N, northwest anomalies over the central and eastern part of the tropical South Atlantic, and westerly anomalies around the equator, suggesting anomalously weak southeast trades accompanied by anomalously strong northeast trades. This wind pattern corresponds to negative SST anomalies in the west and central part of the tropical North Atlantic and positive SST anomalies within 15°S–5°N. The SVD time series of these two variables (Fig. 5b) are highly correlated with each other (correlation coefficient 0.9), generally showing negative values during 1980–83 and positive values during 1984–88 with a temporary weakening in 1987. The variation of the mode is generally out of phase with the DP indices of both the SST and the zonal wind stress.

The heterogeneous map of the second SVD mode (Fig. 6a) shows southwest wind anomalies over the tropical North Atlantic and northwest wind anomalies over the tropical South Atlantic Ocean, implying a simultaneous weakening of both the northeast and southeast trades. Correspondingly, the whole tropical Atlantic basin is warmed up with maximum anomalies in the subtropics. The SVD time series of both variables are also highly correlated with each other (correlation

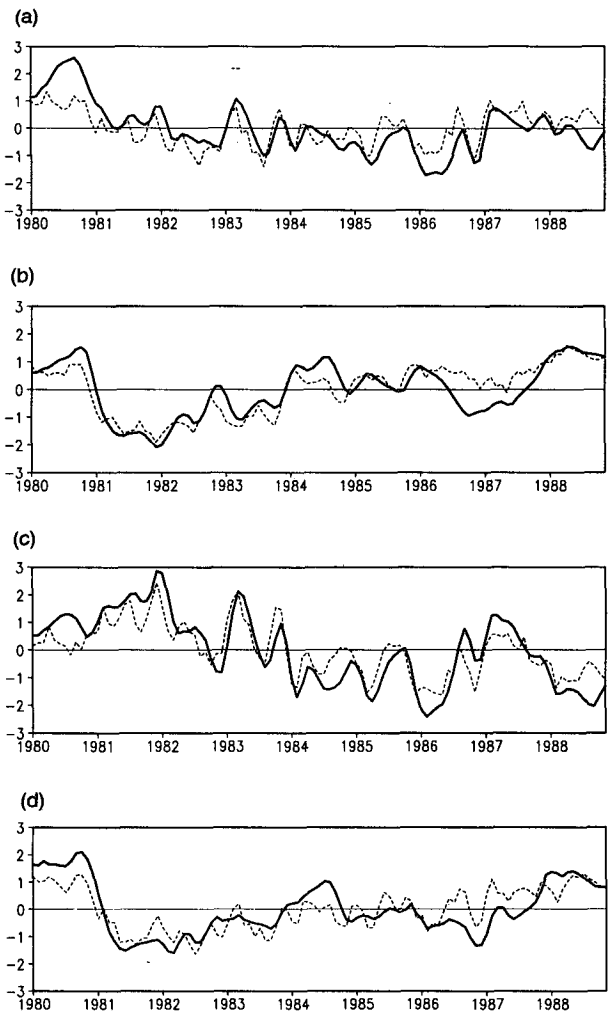

FIG. 4. Indices of zonal wind stress (thin dashed curves) and SST (heavy solid curves) anomalies characterizing the dominant modes of the interannual variability in the tropical Atlantic Ocean for the (a) NB index, (b) SB index, (c) DP index, and (d) TB index.

coefficient 0.85). Both series show fluctuations of large amplitudes during 1980–81, followed by a trend during the rest of the years, which is similar to the TB index of the anomalous zonal wind stress and possibly reflects the error of the wind data in the early 1980s. This mode accounts for 20% of the total covariance. Higher SVD modes are not discussed because they explain much less total covariance of SST and the wind stress.

We propose that the variability of the simulated SST DP index during 1980–88 is forced by the variation of the anomalous wind stress, which also shows a dipole pattern (or meridional gradient near the equator) in the zonal component (Fig. 4c). According to the first SVD mode, the SST DP fluctuation is a manifestation of opposite SST anomalies between hemispheres, forced by an opposite fluctuation of the trade winds. In general, SST is colder in the hemisphere where the surface wind stress is strong. On the other hand, the association of TB indices for SST and zonal wind stress anomalies are more complicated (Fig. 4d). They do exhibit consistent development in the beginning and on a long-term trend, which is also shown in the second SVD mode (Fig. 6). On the other hand, the basinwide warming and cooling after 1984 do not seem to be associated with basin-averaged zonal wind. The structure of the first SVD mode, which exhibits the SST dipole, is derived without the constraint of spatial orthogonality. However, there may exist a possibility that the sampling could result in modal degeneracy in the SVD calculation since the time series are relatively short and the singular values of the two leading modes have similar magnitudes (North et al. 1982). This may introduce uncertainty into the result. Longer simulations are needed to further justify it.

Although the SVD analysis shows that SST anomalies in the central and western part of the ocean are highly correlated with the wind forcing, the standard deviation of the SST anomalies from the simulation (Fig. 7a) shows that the largest SST fluctuations occur near the eastern coast and in the eastern equatorial ocean, where the amplitude can be as high as 1.5°C. Examining the simulated SST anomalies, we found that the off-equatorial anomalies in the central and western part of the ocean usually do not originate locally but move from the east. Average SST anomalies within the regions of large standard deviation (the shaded area in Fig. 7a) are plotted together with the corresponding observations in Figs. 7b,c,d, which represent variations around the eastern coast in the northern (SST1) and southern (SST2) Atlantic Ocean and the eastern equatorial ocean (SST3).

Compared with their corresponding observations, the model reproduced not only the low-frequency variations but also variations on shorter (year to year) timescales for SST1 and SST2 except for the errors in the early 1980s as discussed before (Fig. 7b,c). Considering the lower-frequency fluctuations, SST2 was generally increasing during 1981–88, with negative anomalies in 1981–83 and positive anomalies in 1984–88, whereas SST1 decreased during 1980–86, with positive values in 1981–83 and negative values in 1984–87. Large differences between the simulation and the observation are found for SST3 (Fig. 7d), where the model fluctuations have larger amplitude than the observations. It should be noted that SST3 is averaged over the area with maximum mean error in SST (Fig. 1b) and may reflect the systematic error in the model thermocline near the equator.

Previous studies have suggested that SST anomalies in the east are possibly forced remotely. Based on a correlation analysis of the observed data, Servain et al. (1982) showed that the SST anomaly in the Gulf of Guinea tends to follow the anomaly of the zonal wind stress in the western equatorial ocean. Hirst and Hastenrath (1982) also found that the

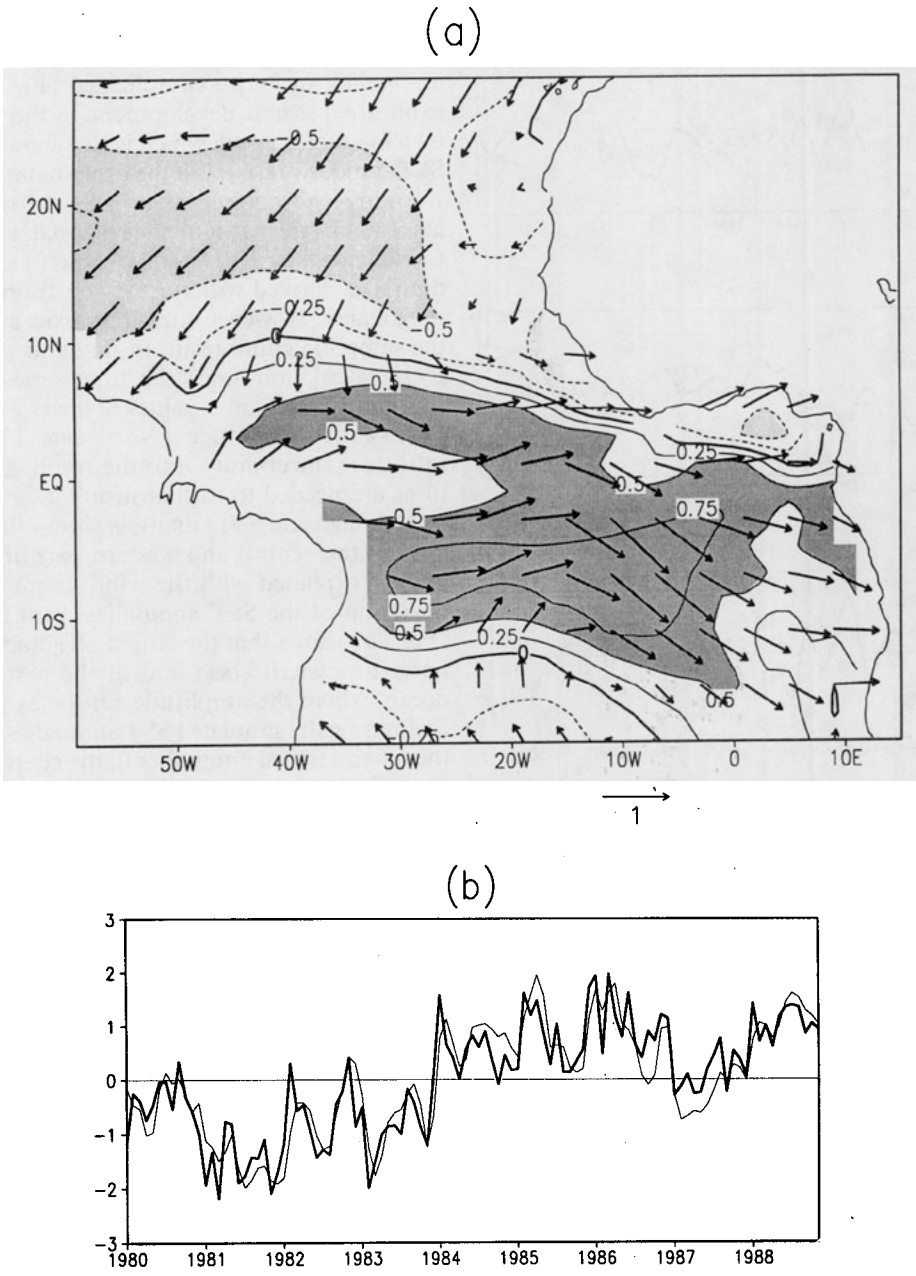

FIG. 5. The first SVD mode of the normalized surface wind stress and SST anomalies for (a) the spatial pattern and (b) the time series. The heavy line in (b) is for the wind stress; the thin curve is for the SST. The contour interval in (a) is 0.25. Regions within 0.5 contour lines have dark shading and regions within −0.5 contour lines have light shading.

anomalous seasonal relaxation of the easterly wind stress over the western equatorial Atlantic remotely forces SST departures in the eastern South Atlantic. In the simulation, SST2 shows large positive correlation with the zonal component of the wind stress in the equatorial Southern Ocean between 0° and 10°S (Fig. 8a) and negative correlation with the meridional wind south of the equator from the east coast to 15°W (Fig. 8b), which suggests that both local and remote forcings play a role in producing SST fluctuations in the eastern coast. The correlation between SST1 and the wind stress anomalies, however, is largest over the eastern tropical Atlantic, showing that weaker (stronger) than normal northeast trade winds are associated with warmer (colder) SST in the eastern part of the northern tropical Atlantic

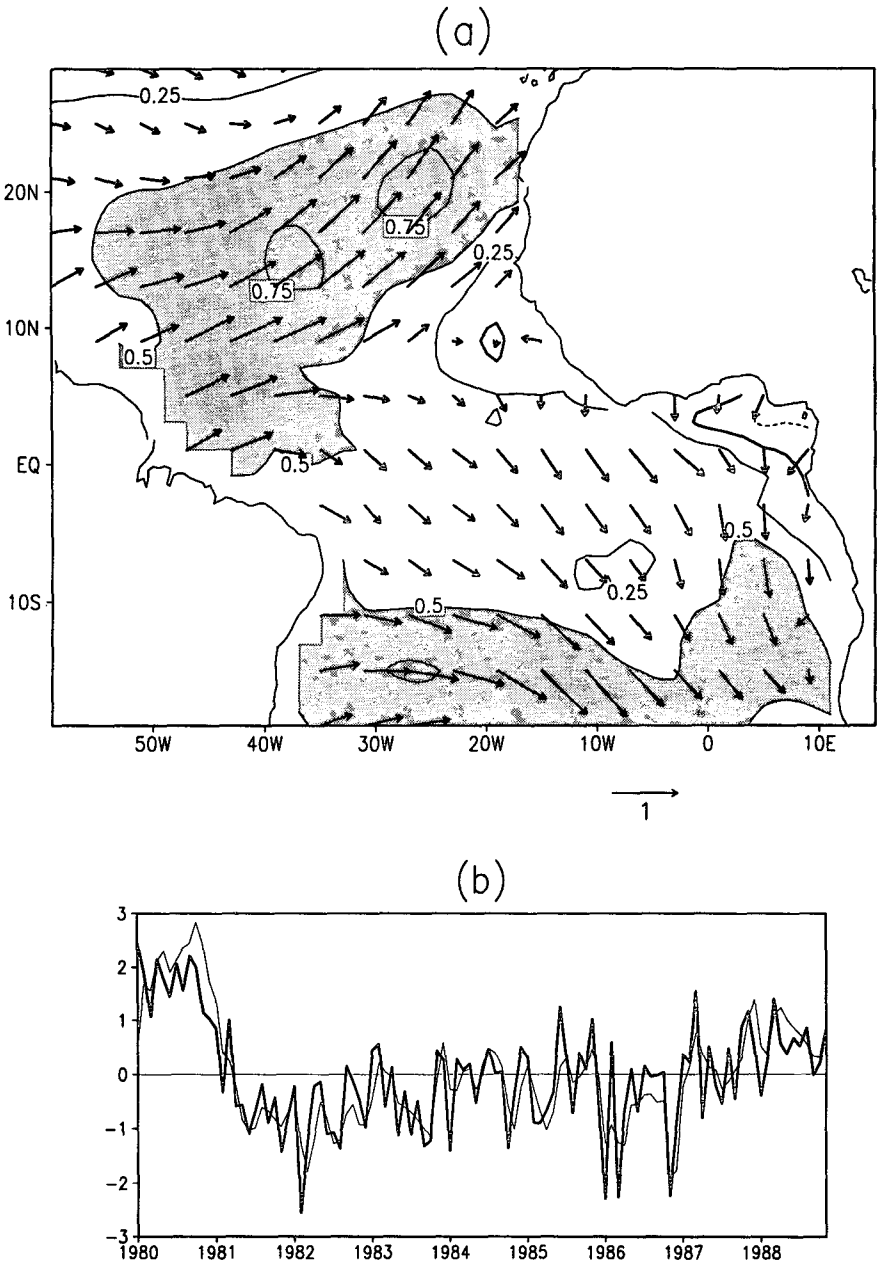

FIG. 6. The second SVD mode of the normalized surface wind stress and SST anomalies for (a) the spatial pattern and (b) the time series. The heavy line in (b) is for the wind stress; the thin curve is for the SST. The contour interval in (a) is 0.25. Regions within 0.5 contour lines have dark shading and regions within −0.5 contour lines have light shading.

Ocean, probably through upwelling induced by the alongshore component of local winds (Figs. 8c,d).

4. Heat content

In this section, we present evidence showing that equatorial wind anomalies can affect the Southern Ocean as suggested by Servain et al. (1982) and Hirst and Hastenrath (1983) and that the SST variability in the eastern ocean south of the equator is a manifestation of basinwide adjustment of the tropical ocean to wind changes. Theoretically, an anomalous zonal wind change along the equator induces a disturbance in the depth of the equatorial thermocline, which propagates eastward (O'Brien et al. 1978; Moore et al. 1978; Weisberg and Tang 1987). What we are going to examine here is how effective this equatorial process is in producing changes in the

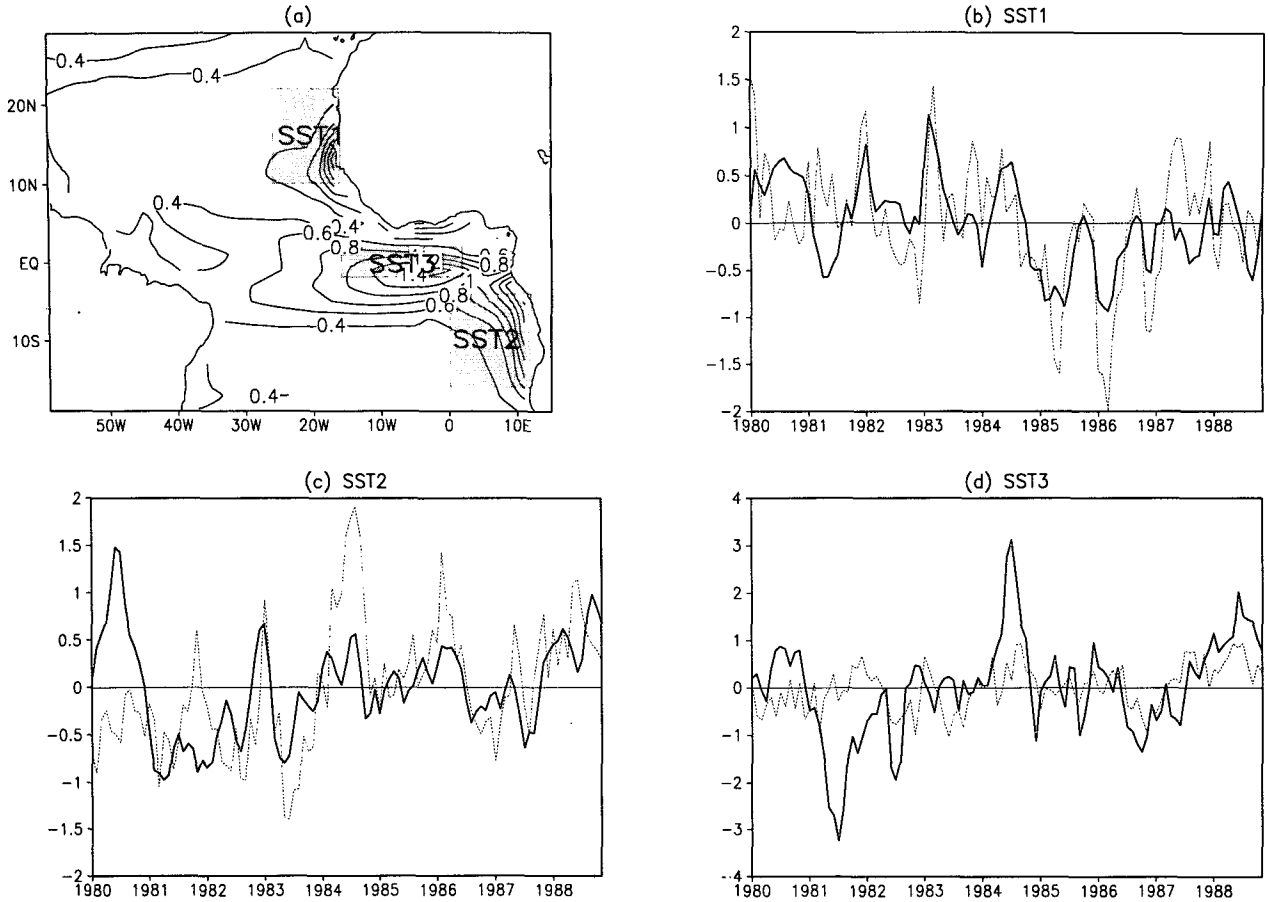

FIG. 7. (a) Standard deviation of the simulated SST monthly anomalies in 1980–88 with contour interval 0.2°C. The shaded areas are regions where the indices SST1, SST2, and SST3 were defined. The simulated and observed indices in 1980–88 are in (b) for SST1, (c) for SST2, and (d) for SST3. The simulation is represented by the solid curve and observations by the dashed curve.

equatorial and the southern eastern ocean. For this purpose, we examine the basinwide thermocline fluctuations.

SST is usually not an appropriate quantity to characterize the depth of the thermocline in the Tropics. In fact, the latter is more closely related to the mean temperature averaged over a depth of the upper ocean. To characterize the changes of thermocline, we have used the ocean heat content (HC) defined as

$$HC = C_P \int_{-H}^{0} \rho_0 T dz, \qquad (1)$$

where $C_P = 3.99\ J°C\ g^{-1}$ is specific heat content $\rho_0 = 1\ g\ cm^{-3}$. The vertical integration is over the upper 300 m ($H = 3 \times 10^4$ cm) including the mixed layer and the thermocline in the Tropics. To the lowest order, the low-frequency variations in surface dynamic topography, sea level, and the depth of the thermocline are equivalent to that of HC. The SST and heat content are correlated in the eastern part of the ocean (Carton and Huang 1994).

a. Annual cycle

The simulated mean state of HC (Fig. 9a) shows alternating highs and lows in the meridional direction that are closely associated with the zonally directed currents through geostrophic balance, which dominates the dynamical balance of forces except very near the equator. For example, between the high values at about 20°N and low values at about 10°N lies the North Equatorial Current. Farther to the south, at about 2°–3°N, high HC is bordering the southern limit of the North Equatorial Counter Current (NECC). Superimposed on the meridional structure are gradients in the zonal direction extending from lower values in the east and higher values in the west for most of the tropical ocean.

We have compared this simulated heat content distribution with the one from the observed climatological temperature distribution (Fig. 9b). The observed climatological temperatures are constructed by Levitus (1982, 1984) based on monthly objective analyses on a composite of station data, expendable bathyther-

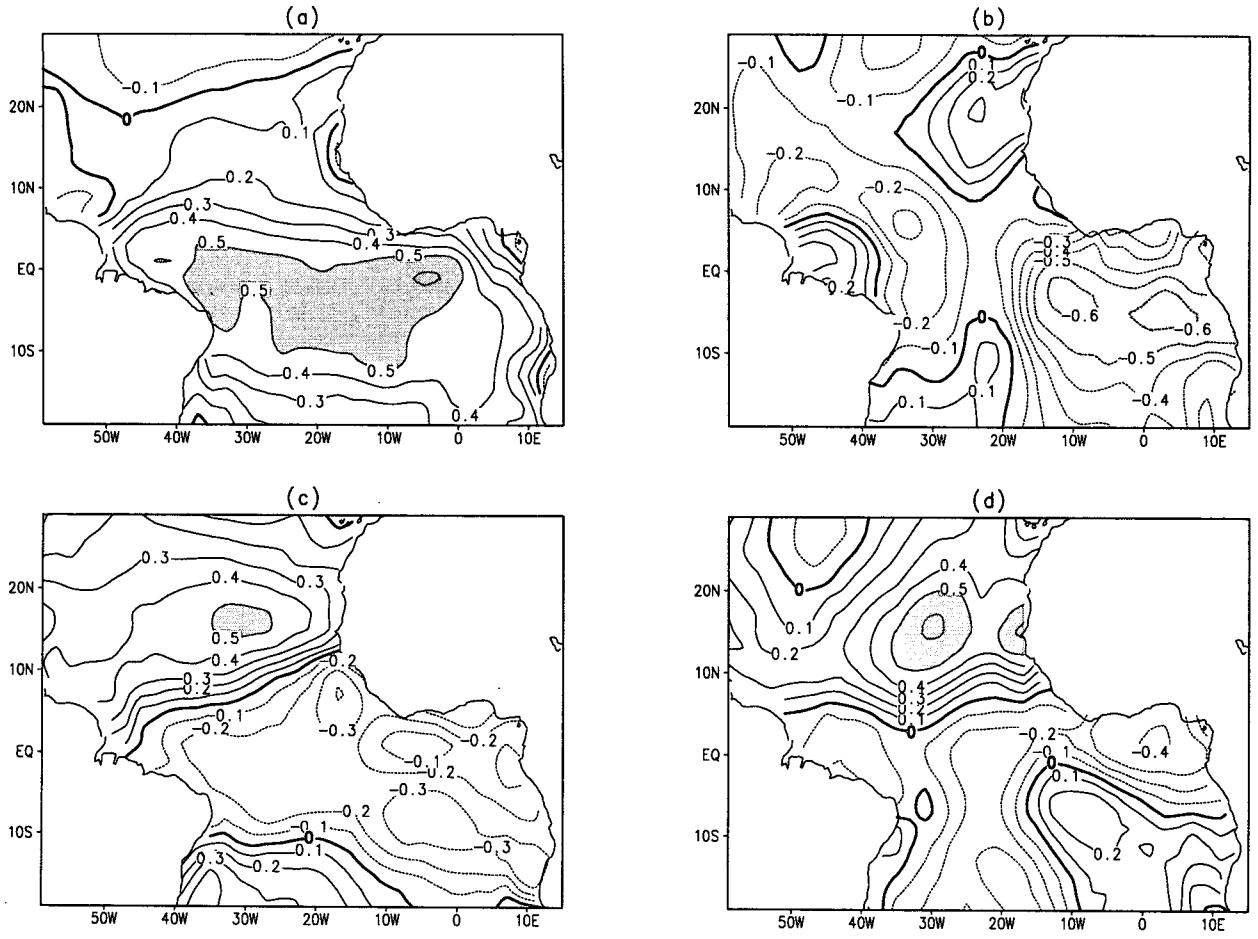

FIG. 8. Correlations between the area-averaged SST anomalies and anomalous wind stress fields: (a) zonal wind stress and SST2, (b) meridional wind stress and SST2, (c) zonal wind stress and SST1, and (d) meridional wind stress and SST1. The contour interval is 0.1 for all the maps. The significance level for 99% confidence is 0.25. Regions with correlation greater than 0.5 have dark shading and regions with correlation less than −0.5 have light shading.

mograph data, and mechanical bathythermograph data on file at the National Oceanographic Data Center. The original data are global on a 1° × 1° grid on chosen vertical levels with intervals increasing from 10 m near the surface to 50 m around the depth of 300 m. The temperatures are interpolated to the model grid point before being integrated into heat content. The pattern of the simulated mean heat content is realistic in comparison with the climatological HC distribution from observed climatological heat content, although the gradients are too weak to the north.

The heat content within the basin is seasonally redistributed due to surface wind changes. In boreal autumn (Fig. 10a), heat content is maximum to the north of the equator in the western ocean in association with strong southeast trade winds and the northernmost position of the ITCZ. With the weakening of the trade winds along the equator in boreal winter (Fig. 10b), some of the heat is transferred across the ocean along the equator, starting the seasonal deepening of the thermocline in the Gulf of Guinea. At the same time heat content increases in the western ocean south of the equator. In boreal spring (Fig. 10c), when the ITCZ is closest to the equator so that wind is relatively weak there, the thermocline is quite flat along the equator as seen by negative HC anomalies in the west and positive HC anomalies in the east. This situation changes in association with the strengthening of easterly winds in the equatorial region in boreal summer (Fig. 10d), which causes shoaling of the thermocline in the Gulf of Guinea and positive HC anomalies to the west off the equator. This pattern of simulated seasonal cycle of HC is in agreement with the observations (Huang 1992).

b. Interannual variability

Figure 11a shows the standard deviation of monthly mean HC anomalies. High HC variability appears in the western ocean off the equator both to the north

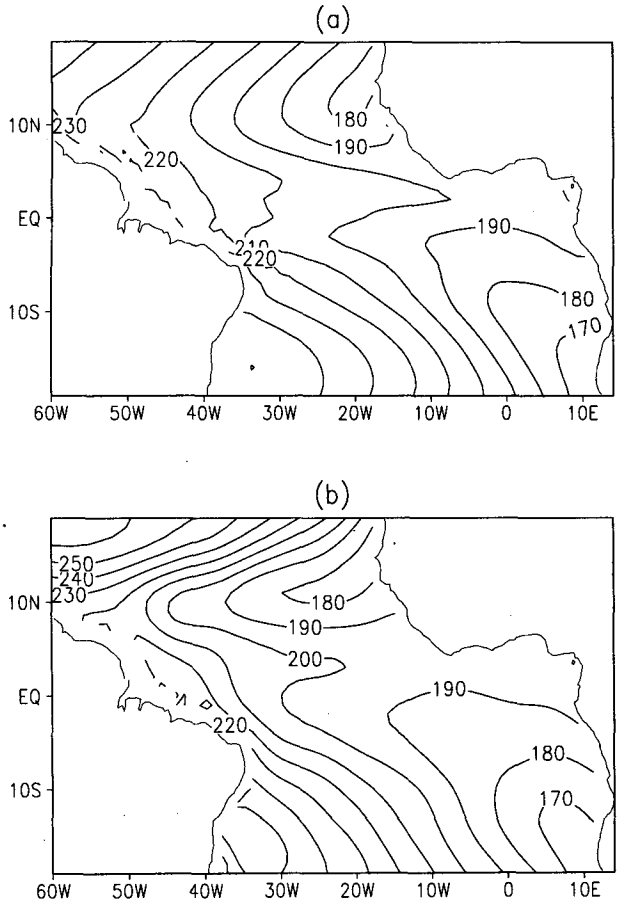

FIG. 9. Climatological mean fields of the upper-ocean heat content from (a) the simulation and (b) observations. Contour unit is 10^4 J cm^{-2}.

and south, and in the eastern coast mostly to the south of the equator off the African coast. The regions of high HC variability coincide with the locations of the largest HC amplitude in the annual cycle. The time series of the HC (Fig. 11b) in regions of highest variability in the western ocean, referred to as H1 and H2 for the northern and southern centers, show remarkably similar behavior to the north and south of the equator. It can be seen that the HC was high (the thermocline is very deep) during 1981–83, but decreased rapidly in early 1984 and remained low during 1985–86. Then, after briefly returning to normal in the summer of 1987, it decreased again in late 1987–88. Interestingly, HC fluctuations in the eastern coast to the south of the equator (H3) show an almost complete out-of-phase relationship with H1 and H2 (Fig. 11c).

This nearly out of phase relationship between the low-frequency HC variations in the eastern coast to the south of the equator (H3) and those in the western tropical ocean (H1 and H2) implies that heat is transferred across the basin on interannual timescales. Carton and Huang (1994) from the model-simulated equatorial warm events in the tropical Atlantic Ocean have identified positive HC anomalies moving from the western ocean to the Gulf of Guinea through the equatorial waveguide during 1983–84 and 1987–88 warm events. The result here shows that these displaced HC anomalies can be maintained for a relatively long period, causing an out of phase low-frequency fluctuation between the eastern and western ocean in the Tropics.

This relationship between HC anomalies and surface wind stress can be shown using the statistical technique of the extended EOF analysis. Denoting a temporarily changing field of N spatial points by an N-dimensional state vector $X(t)$, the conventional EOF analysis extracts the modes that account for maximum fractions of its total variance, which is accomplished by solving for the leading eigenvalues and corresponding eigenvectors of the $N \times N$ covariance matrix of $X(t)$. In practice, such an analysis is more appropriate for stationary rather than for propagating patterns. An extension of this method (called as extended EOF) combines the spatial and temporal information to describe propagating features. In essence, this is done by expanding the state vector with data from adjacent times (e.g., see Weare and Nasstrom 1982).

In the present case, both the heat content and wind stress anomalies, divided by their corresponding mean standard deviations, are combined together as an $X(t)$ for the extended EOF analysis. A detailed discussion of combining variables for an EOF analysis is given by Kutzbach (1967). Then, a new state vector $Y(t)$ is formed by padding four consecutive fields of $X(t)$ into $Y(t) = [X(t), X(t+6), X(t+12), X(t+18)]$, with $X(t+6)$ lagging $X(t)$ by six months, and so forth. The maximum time lag (18 months) within a state vector is chosen to match the lifetime of two major warm events in 1983–84 and 1987–88 (Carton and Huang 1994). As in a conventional EOF analysis, the variance maximization procedure for the extended field $Y(t)$ leads to an eigenvalue problem for the $4N \times 4N$ covariance matrix. Each of the resulting $4N$-dimensional eigenvectors may be partitioned into four individual N-dimensional fields, which may in turn be displayed in a series of four successive spatial patterns, each lagging by six months.

The first mode (Figs. 12a–d) shows an HC pattern with three centers in the location of the largest interannual variance (Fig. 11a). The two western centers to the north and south of the equator have the same sign, which is opposite to the eastern center to the south of the equator. The surface wind pattern associated with this HC pattern shows an opposite tendency between the southeast and northeast trades with strong anomalous zonal winds along the equator. The fact that both the HC and the wind patterns do not change much in the four panels suggests that this pattern has a persistence longer than two years and represents a stationary response of the upper ocean to the winds.

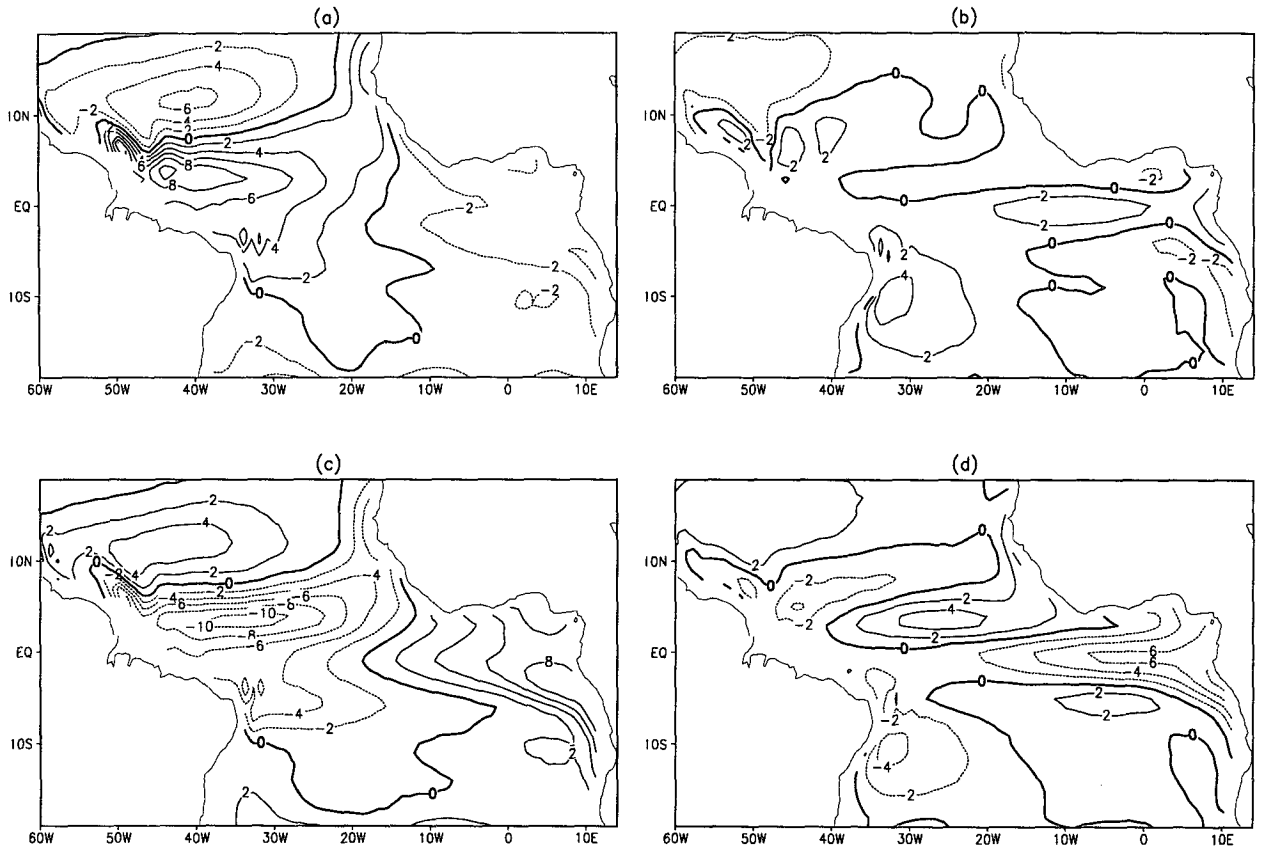

FIG. 10. Seasonal cycle of the simulated upper ocean heat content for (a) autumn, (b) winter, (c) spring, and (d) summer, with contour interval 2×10^4 J cm^{-2}. The annual mean has been subtracted from the seasonal cycle.

Also notice the similarity of this wind stress pattern with the one presented in the first SVD pattern of the wind stress and SST anomalies (Fig. 5a).

The time series of this mode (solid line, Fig. 14) has opposite signs between 1981–83 and 1985–86, which is also similar to the variation of the DP indices. With this mode, the thermocline was deep in the western ocean both to the south and north of the equator but shallow in the Gulf of Guinea and off the Angola coast during 1981–83 when the southeast trades were strong and the easterlies were intense on the equator. During 1985–86, however, both the wind and HC patterns were reversed.

The second mode exhibits how this reversal is realized (Fig. 13). The sequence of the spatial maps starts from a state similar to the one shown by the first mode for both the anomalous HC and the southeasterly trade winds, but the anomalous northeast trades are reversed (Fig. 13a). Six months later, as the zonal wind anomalies become negligible along the equator, the large HC anomaly off northeast Brazil is weakened, accompanied with an HC increase in the east (Fig. 13b). At 12 month's lag (Fig. 13c), anomalous westerly winds prevail around the equatorial ocean and HC increases in the eastern equatorial ocean and along the African coast intensively. Positive HC anomalies in the western ocean have been replaced by negative centers. Finally, at 18 month's lag (Fig. 13d), as weak southeast trades and equatorial anomalous westerlies are established, HC anomalies are negative in the western ocean off the equator and positive in the Southern Ocean. The last panel basically can be seen as the first panel with the signs of the contours and the directions of the winds in the south reversed. The time series (dashed line, Fig. 14) shows that this mode was most active during 1983—84 when a transition of phase in the first mode occurred.

The EOF analysis shows that the interannual variations of the thermocline in the tropical Atlantic Ocean are closely related to the interannual fluctuations of the trade winds and zonal winds along the equator. It seems that the interannual change of the zonal winds around the equator plays two roles. First, it changes the slope of the thermocline along the equator. Second, the anomalous meridional gradient of the zonal winds associated with the wind fluctuation along the equator affects the heat exchange between the equatorial and off-equatorial regions. Theoretically, local wind curls induce an Ekman pumping velocity w_e, which changes the depth of the thermocline H_m as

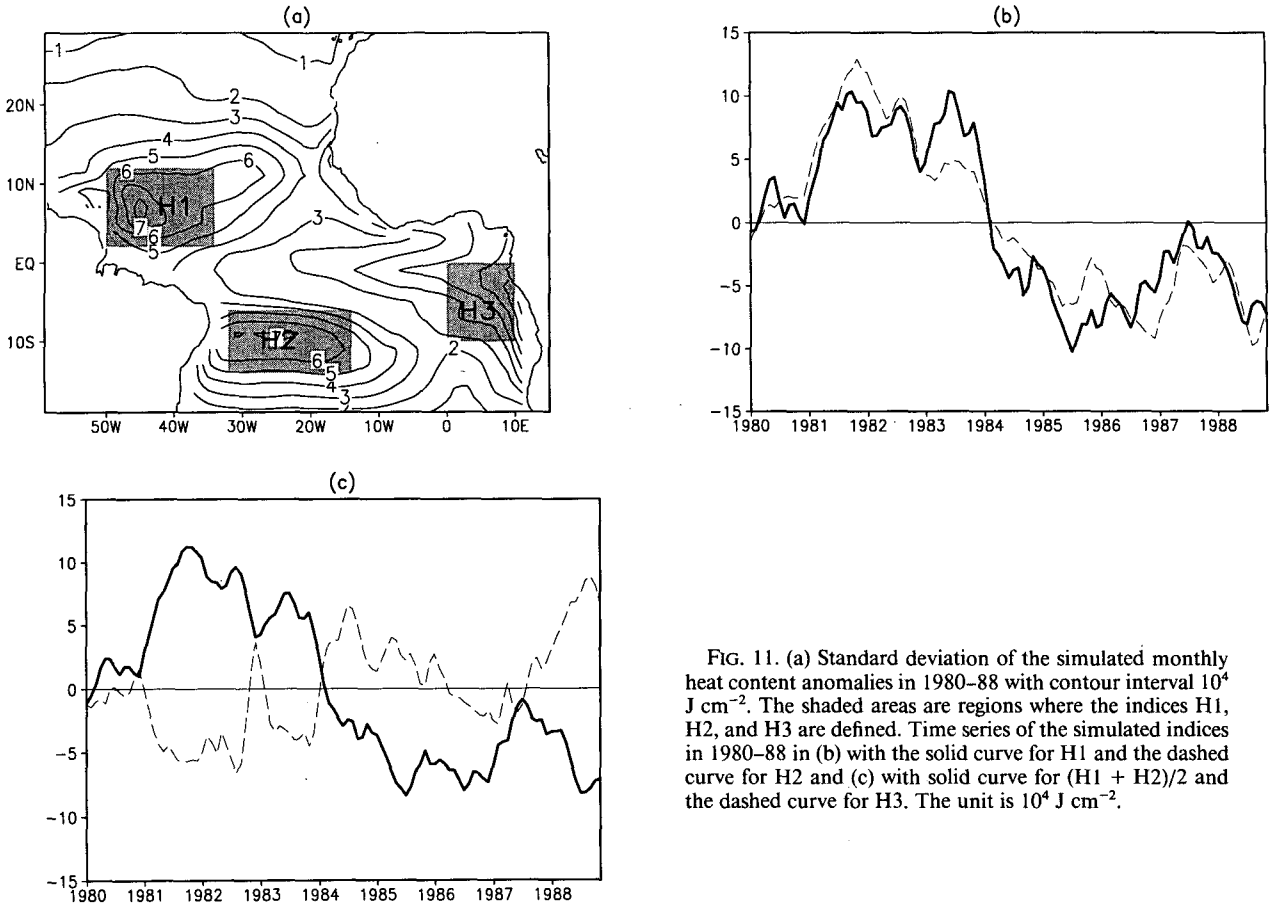

FIG. 11. (a) Standard deviation of the simulated monthly heat content anomalies in 1980–88 with contour interval 10^4 J cm^{-2}. The shaded areas are regions where the indices H1, H2, and H3 are defined. Time series of the simulated indices in 1980–88 in (b) with the solid curve for H1 and the dashed curve for H2 and (c) with solid curve for (H1 + H2)/2 and the dashed curve for H3. The unit is 10^4 J cm^{-2}.

$$w_e = \mathbf{k} \cdot \nabla \times (\tau/\rho_0 f) \quad (2)$$

$$\partial H_m/\partial t \sim -w_e, \quad (3)$$

where $f = 2\Omega\sin\phi$, and the unit of w_e is centimeters per second. Therefore, high negative correlation is expected between the time derivative of H_m and w_e if the effect of local wind curls dominates. Actually, negative correlation between the tendency of the anomalies of the 20°C isotherm depth and w_e is found around the two major centers of HC anomalies in the western ocean to the north and south of the equator (Fig. 15). This suggests that when the easterlies were strong in 1981–83, water was pushed out of the equatorial ocean through anomalous Ekman transport, which deepens the thermocline to the south and north of the equator. However, when the easterlies were weak in 1985–86, water moved back to the equatorial region.

The pattern of heat content anomalies in the western tropical Atlantic Ocean and its relationship with surface wind forcing, as revealed by the EOF analysis, are qualitatively similar to those found in the western tropical Pacific Ocean. For example, Philander and Hurlin (1988) and Zebiak (1989) emphasized the importance of the meridional heat transports near the equator for El Niño events and ENSO-like oscillation in the coupled atmosphere–ocean models (e.g., Zebiak and Cane 1987). Barnett et al. (1991) and Chao and Philander (1993) have also noted that the westerly wind anomalies over the western equatorial Pacific during warm events (El Niño) elevate the thermocline in the west, especially off the equator where the curl of the wind is large. It is conceivable that, as in the Pacific Ocean, the off-equatorial elevations generated by wind anomalies in the western Atlantic would disperse into Rossby waves and equatorial Kelvin waves. At the western coast, the Rossby waves may be reflected as equatorial Kelvin waves to elevate the thermocline in the east and induce an oscillation, such as suggested by the "delayed oscillator" mechanism for ENSO (Schopf and Suarez 1988; Suarez and Schopf 1988; Battisti and Hirst 1989).

However, as noted by Zebiak (1993), a direct application of the delayed oscillator mechanism in terms of single-wave modes may lead to a much shorter oscillation period in the Atlantic than in the Pacific Ocean, given the smaller zonal dimension of the At-

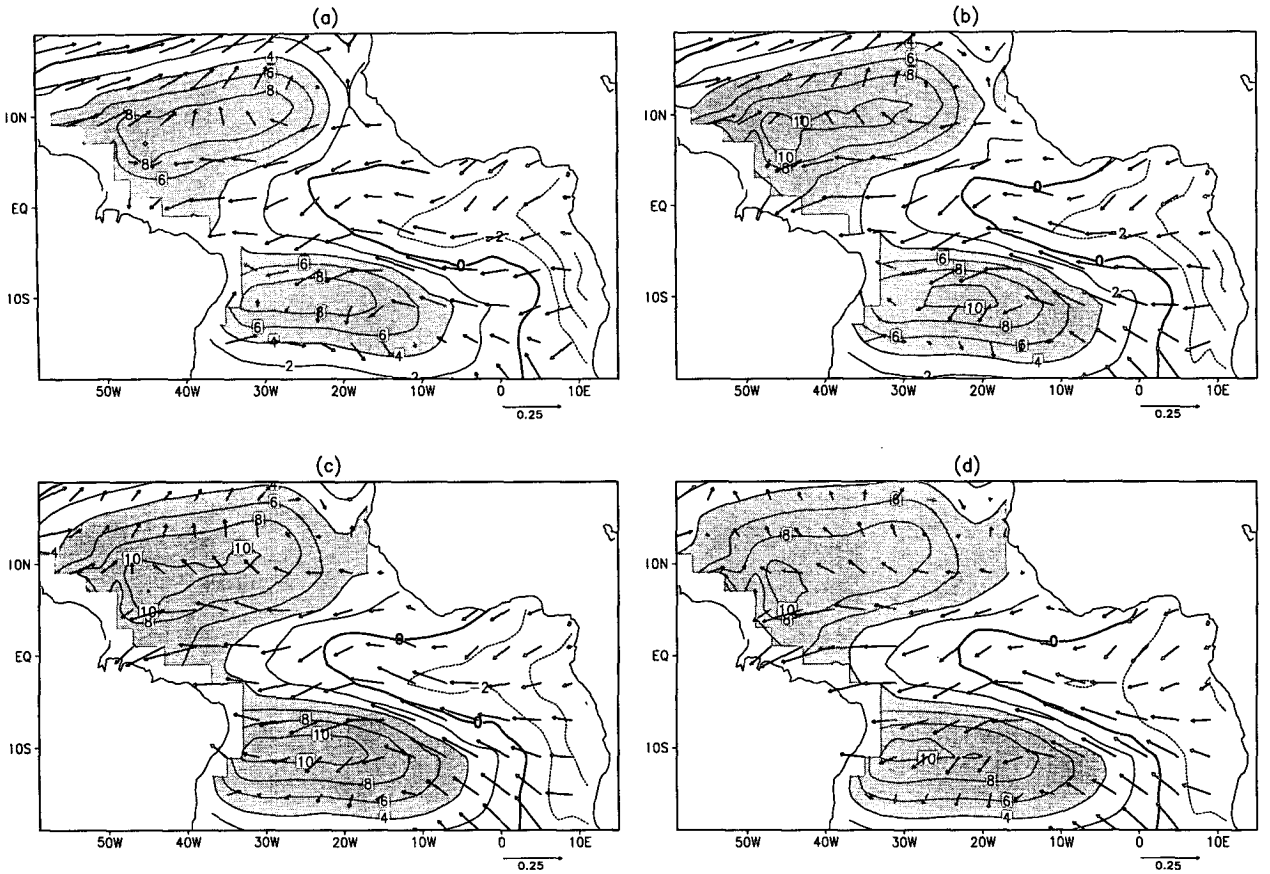

FIG. 12. The spatial patterns of the first extended EOF combining the anomalous wind stress and the simulated anomalous upper ocean heat content. The vector-formatted surface wind stress is shown atop the contours of the heat content. The spatial patterns are (a) at a given time t, (b) $t + 6$, (c) $t + 12$, and (d) $t + 18$. The unit of time increment is month; arrows at bottom right of each plot correspond to 0.25 dyn cm^{-2}; contour interval for the heat content is 1×10^4 J cm^{-2}. Regions with HC anomalies greater than 2×10^4 J cm^{-2} have dark shading, and regions with anomalies less than -2×10^4 J cm^{-2} have light shading. This EOF mode accounts for 28% of the domain-averaged variance of the combined data.

lantic, although in observation the equatorial Atlantic shows dominant oscillation periods similar to the Pacific. Therefore, a modified "delayed oscillator" mechanism (Chao and Philander 1993), which emphasizes that at any moment not single-wave modes but the total delayed oceanic response to earlier winds causes a continual oscillation, may be more appropriate here. In comparison with the tropical Pacific, there is one more complexity in explaining the Atlantic variability: the equatorial wind fluctuations are not purely caused by air–sea interactions within the tropical Atlantic domain; outside effects may play an equally or more important role (Horel et al. 1986).

In the eastern part of the tropical Atlantic Ocean, heat content anomalies show asymmetry with respect to the equator although they are symmetric in the west. Heat content anomalies transferred from the western ocean tend to move to the southern part of the ocean, possibly due to the geometry of the eastern Atlantic basin or the mean state of the ocean. This fact may have important implications for the origin of the dipolelike SST fluctuations in the tropical Atlantic Ocean since the SST and heat content anomalies are highly correlated in the east. It is not just a coincidence that the transition of the phase of SST DP index started in 1983-84 when the unprecedented anomalous warm event occurred in the eastern ocean. It was during this warm event that heat content anomalies moved to the southern part of the eastern ocean, which affected the SST there. The SST anomalies then moved westward and remained in balance with the wind in the central part of the ocean.

5. Circulation and transport

The simulated mean currents are qualitatively similar to the observations (Richardson and McKee 1984) and a simulation by Philander and Pacanowski (1986b, hereafter PP) with monthly climatological wind stress (Hellerman and Rosenstein 1983). Quantitatively, the

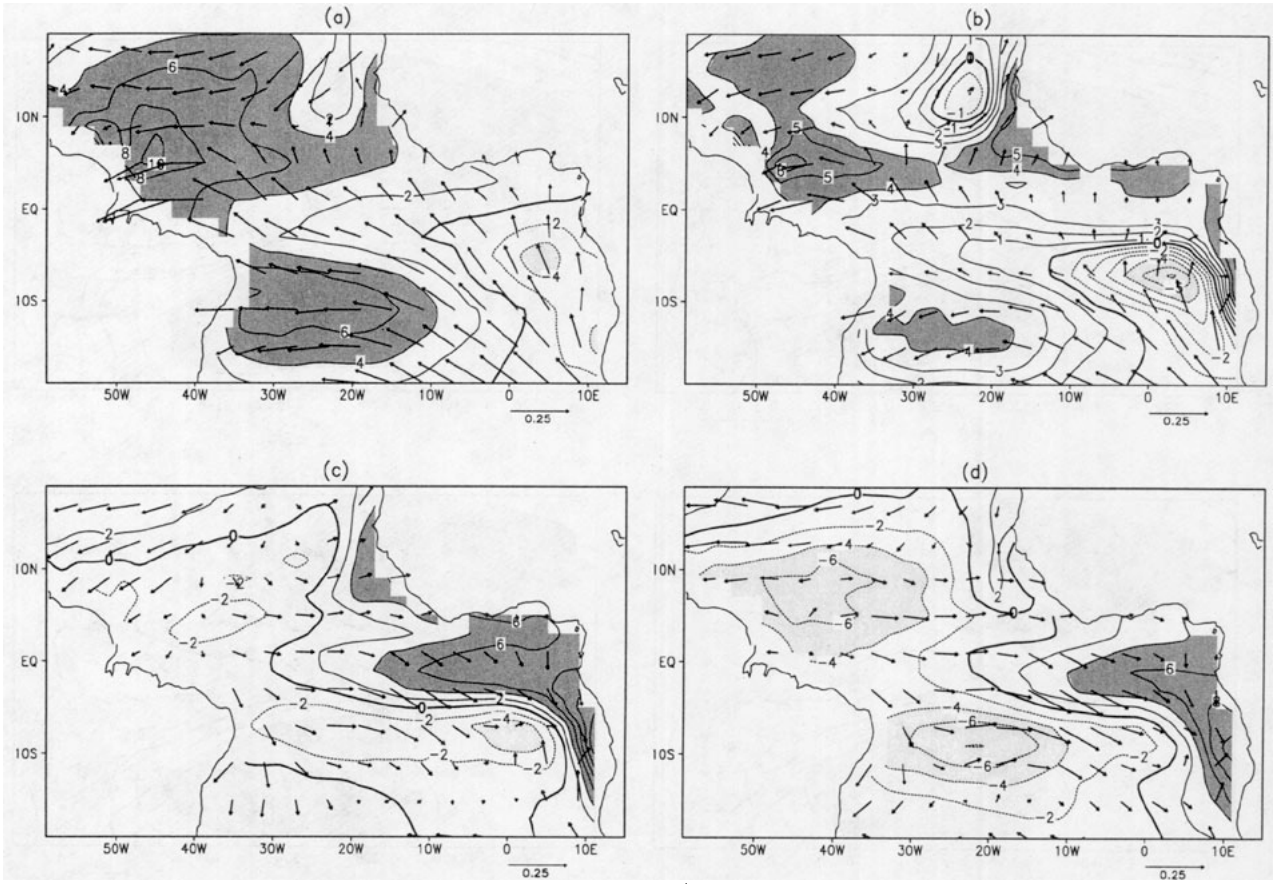

FIG. 13. The spatial patterns of the second extended EOF combining the anomalous wind stress and the simulated anomalous upper-ocean heat content. The vector-formatted surface wind stress are shown atop the contours of the heat content. The spatial patterns are (a) at a given time t, (b) $t + 6$, (c) $t + 12$, and (d) $t + 18$. The unit of time increment is month; arrows at bottom right of each plot correspond to 0.25 dyn cm^{-2}; contour interval for the heat content is 2×10^4 J cm^{-2}. Regions with HC anomalies greater than 2×10^4 J cm^{-2} have dark shading and regions with anomalies less than -2×10^4 J cm^{-2} have light shading. This EOF mode accounts for 9% of the domain-averaged variance of the combined data.

surface South Equatorial Current (SEC) velocities from this and PP's simulations are both about 10 cm s^{-1} stronger than surface measurements from ship drifts (Richardson and Philander 1987), which is about the level of accuracy for the measurements. However, the surface velocity of the North Equatorial Counter Current (NECC) from our simulation is weaker, whereas the one from PP's simulation is stronger than the observations, which may be attributed to the differences of the wind forcings. The magnitudes of mean Equatorial Under Current (EUC) are comparable in both runs. The annual cycles of the two simulations are also similar, as measured by the transport at 30°W.

The interannual fluctuations of the tropical currents in 1980–88 from our simulation were closely related to the interannual fluctuations of the oceanic thermal structure as well as the wind stress. Anomalous transports by SEC and EUC at 30°W show low-frequency variability consistent with the anomalous wind and heat storage in the Tropics. Transports by both currents were intensified in 1981–83 when the equatorial easterly winds were stronger and were weaker in 1985–86 and 1988 when the easterly winds were weaker (Fig. 16a). They also had opposite signs and tended to balance each other most of the time. These variations reflect the changes in the slope of the thermocline along the equator associated with the fluctuations of the thermal structure of the upper ocean. In 1981–83, the thermocline was steeper and the zonal pressure gradient was larger; in 1985–86, the situation was reversed.

The NECC transport was anomalously large in 1983 and 1987 but small in 1980 (Fig. 16b). The strengthenings are associated with the HC peaks in 1983 and 1987 in the western ocean (H1 in Fig. 11b) and should be related to the fluctuations of the meridional slope of the thermocline between 3° and 10°N. The positive peaks of NECC preceded the simulated warm events in the eastern ocean, implying strong links between the equatorial and the northern ocean, before an eastward shift of heat content (Carton and Huang 1994). The

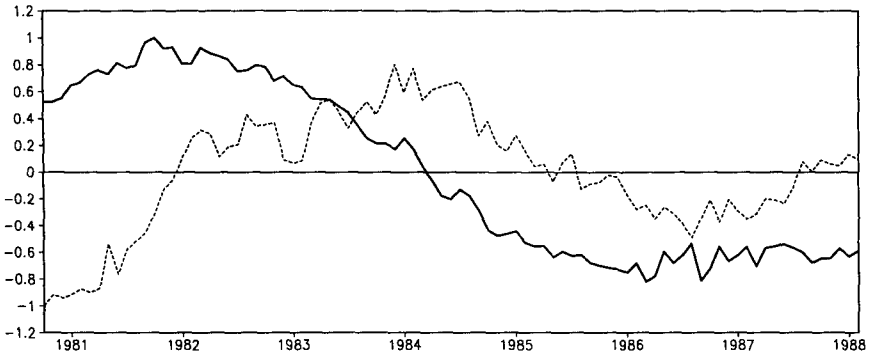

FIG. 14. The first (solid line) and second (dashed line) of the principal components of the extended EOF modes of the surface wind stress and heat content anomalies. The curves are normalized by their maxima. The curves are plotted with time corresponding to the midpoint of the four instances within an expanded state vector.

strengthening of NECC in 1983 and 1987 in the tropical Atlantic Ocean was observed from inverted echo sounder measurements of heat content (Katz 1993). However, considering the problems in wind stress data during 1980–81 as discussed in section 3, the interannual fluctuations of the simulated currents described here may not be realistic for this period.

As described in PP, the currents affect each other through water transport. The North Brazil Current (NBC) receives flow from the westward SEC and in turn feeds the eastward EUC and the NECC. During its eastward movement, the NECC loses water into the thermocline, which merges southward to the EUC. The EUC in turn loses water to the SEC in equatorial upwelling giving rise to a meridional cell that develops with upwelling around the equator and downwelling north of 5°N. We would like to consider this pattern as composed of two interconnected circulations within the tropical Atlantic Ocean: one links the equatorial ocean with the Southern Ocean and the other links it to the north. The one linking the south has basinwide scales, including the northward NBC, eastward EUC along the equator, equatorial upwelling in the east, and the westward SEC. The one linking to the north is more localized, basically composed of the meridional cell linking the upwelling around the equator and downwelling north of 5°N, which involves local water exchange between the NECC, EUC, and SEC in the western ocean.

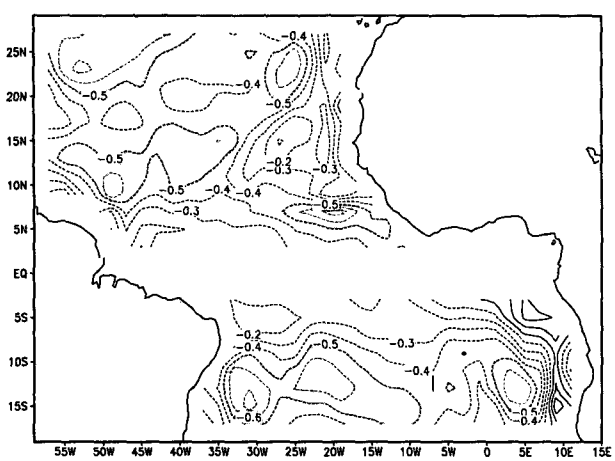

FIG. 15. Correlation between tendency of monthly anomalies of 20°C isotherm depth and the anomalous vertical velocity induced by Ekman pumping at the bottom of the mixed layer. Regions of correlation less than −0.5 shaded. The level of significance with 99% confidence is 0.25.

We have also examined mass transport at several critical regions in the model domain. In the western part of the ocean, the meridional cell formed between the equatorial and northern ocean was more intense in 1981–83 when the easterly winds around the equator were stronger, and weaker in 1985–86 as well as in late 1987–88 when the winds were weaker. On the other hand, transport into the equatorial ocean from the south was also weakened from the former to the latter periods due to the weakening of the SEC and NBC, so was the eastward transport by EUC around the equator. The EUC fluctuation affects the circulation in the east. Actually, in the eastern part of the ocean, anomalous mass transport at the upper 300 m through a cross section at 2.5°S extending from 10°W to the African coast was southward during 1981–83, but in 1984–88 it was northward except for a short period in 1987.

The circulation variability affects the heat transports in the upper ocean. In the mean, zonal heat transport in the upper ocean (0–300 m) at 30°W is eastward near the equator and westward in the south mainly due to EUC and SEC. In 1981–83, when both the EUC and SEC were intense, this transport pattern was strong along the equator. However, it was suddenly reduced in 1984 both around and to the south of the equator. Then it remained significantly weaker during the period 1985–88 (Fig. 17a).

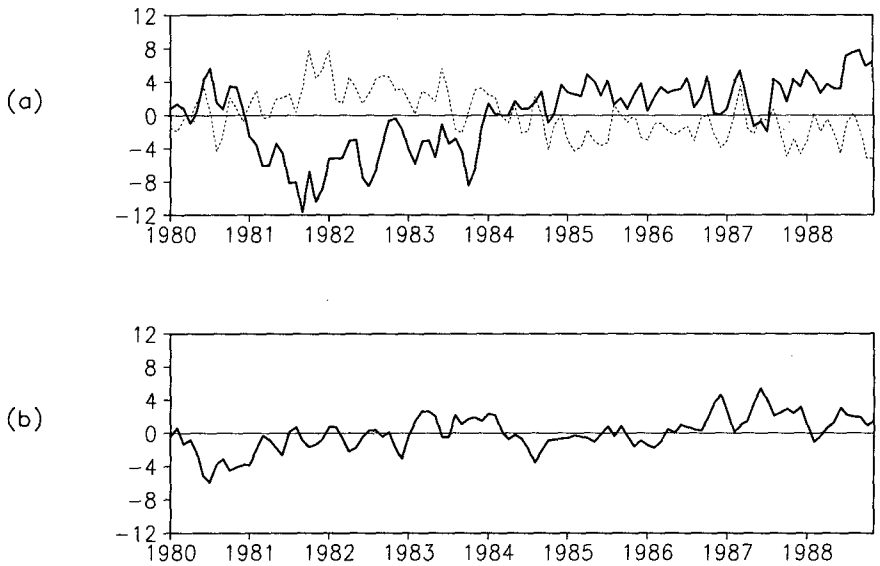

FIG. 16. (a). Transports by the anomalous SEC (thick line) and EUC (thin line) across 30°W above 317 m and between 10°S and 10°N. (b) Anomalous transport by NECC. Positive values indicate anomalous eastward transport. The units are Sv. The anomalies are calculated based on monthly climatology averaged through 1980–88. The transport by SEC is defined as that by westward currents between 10°S and 3°N. The transport by EUC is defined by that due to eastward currents between 10°S and 3°N. The transport by NECC is defined by that due to eastward currents between 3° and 10°N.

The zonally integrated meridional transport is northward in the mean and is mainly affected by the fluctuations of the meridional cell near the equator and NBC near the western coast. In 1981–83, when the meridional cell and transport by NBC into the equatorial ocean was strong, more heat was transported

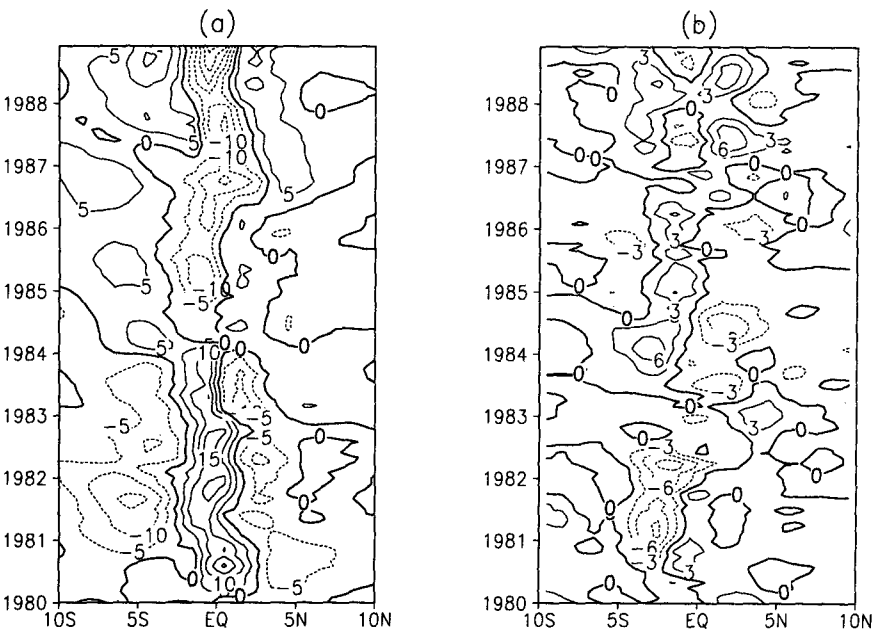

FIG. 17. (a) Anomalous zonal heat transport at 30°W with depth from surface to 300 m. The contour interval is 5×10^8 W m^{-1}. (b) Convergence of zonally integrated anomalous northward heat transport as a function of time and latitude. The contour interval is 3×10^8 W m^{-1}.

from the southern equatorial ocean to the north so that heat divergence was intense to the south of the equator. Starting from 1984, this meridional cell and the NBC transport reduced significantly and there was convergence of anomalous heat to the south of the equator. In 1987–88, another switch of the convergence across the equator occurred (Fig. 17b).

6. Summary and discussion

We have examined the results of a numerical simulation of the variability in the tropical Atlantic Ocean forced by the ECMWF monthly surface wind stress during 1980–88. The mean state and annual cycle of the ocean are realistically simulated by the model. The simulated interannual variability of the SSTs are also remarkably consistent with the observations. The observed dominant SST variability (the basinwide warm/cold periods and the meridional SST gradient near the equator) was reproduced by the model in 1980–88, including the equatorial warm events in 1984 and 1987–88 as well as a major transition of the SST DP index in 1984–85. Major shortcomings of the simulation are excessively cold SST and a shallow thermocline in the eastern equatorial ocean as well as weak NECC in the model mean state. Discrepancies between the observed and simulated SST anomalies in 1980–81 seem to be due to the poor quality of the ECMWF analysis during that period.

According to the SVD analysis, the low-frequency fluctuations of the meridional SST gradient during 1980–88 were a manifestation of opposite SST anomalies between hemispheres, forced by out of phase fluctuation of the trade winds. Specifically, the southeast trade winds were anomalously strong during 1981–83 and weaker than normal during 1985–86 and 1987–88. The northeast trade winds, on the other hand, showed the opposite variation, being weak in 1980–83 and strong in 1984–86. In general, the SST was colder where the surface wind stress was stronger.

SST fluctuations in 1980–88 were associated with profound low-frequency variations of the ocean circulation and thermal structure. The northeast trade winds maintained a local oceanic circulation in the eastern ocean that was composed of upwelling along the coast, advection toward the open ocean, downwelling in the ocean interior, and transport in the subsurface toward the coast. When the tradewinds were weak in 1980–83, this local cell was weak so that upwelling near the eastern coast was suppressed and the SST was raised. When the wind became strong after 1984, the local circulation was intensified so that upwelling was strengthened and the SST was reduced. The warmer (colder) water in the east then moved westward by advection.

On the other hand, the southeast trade winds affect the tropical ocean by generating basinwide changes. The primary factor responsible for differences in the role of the two trade wind stresses is the asymmetry of the wind pattern with respect to the equator. The southeast trade winds extend northward across the equator in the western ocean. However, the northeast trades rarely pass to the south of 5°N. Therefore, the oceanic thermal structure and circulation near the equator were generally influenced by the southeast trade winds. When the southeast trades were strong in 1981–83, the slope of the thermocline was steeper along the equator, both the SEC and EUC were intensified, and the heat content was positive in the western ocean off the equatorial region by strong Ekman transport forced by strong equatorial easterly winds. As a result, the thermocline was shallow in the Gulf of Guinea. The southward transport by the current along the African coast was large and temperature in the eastern ocean south of the equator was low. When the southeast trade winds were weak in 1985–86, the equatorial thermocline was flat and both the SEC and EUC were weaker. The anomalous heat content in the west was transferred to the east and then to the south of the equator, deepening the local thermocline there and making SST warmer. This transfer of heat content from the west to the east was accomplished during 1983–84 when the southeast trade wind started weakening and winds along the equator decreased significantly.

Acknowledgments. Financial support for this research has been provided by the National Science Foundation under Grants ATM-9019296 and OCE-9000060. The numerical simulations were carried out at NCAR CRAY/YMP. We would like to thank Dr. B. Kirtman for comments on the manuscript. We are also grateful to Dr. S. Schubert for providing the ECMWF wind analyses for this study.

REFERENCES

Barnett, T. P., M. Latif, E. Kirk, and E. Roeckner, 1991: On ENSO physics. *J. Climate,* **4,** 487–515.

Battisti, D. S., and A. C. Hirst, 1989: Interannual variability in the tropical atmosphere/ocean system: Influence of the basic state and ocean geometry. *J. Atmos. Sci.,* **46,** 1687–1712.

Bretherton, C. S., C. Smith, and J. M. Wallace, 1992: An intercomparison of methods for finding coupled patterns in climate data. *J. Climate,* **5,** 541–560.

Busalacchi, A. J., 1987: Atlantic seasonality: II Theory. *Further Progress in Equatorial Oceanography. A Report of the U.S. TOGA Workshop on the Dynamics of the Equatorial Oceans, Honolulu HI, August 11–15, 1986.* E. J. Katz and J. M. Witte, Eds., Nova University Press, 235–254.

Cane, M. A., and A. J. Busalacchi, 1987: Atlantic seasonality: III Conclusions. *Further Progress in Equatorial Oceanography. A Report of the U.S. TOGA Workshop on the Dynamics of the Equatorial Oceans, Honolulu HI, August 11–15, 1986,* E. J. Katz and J. M. Witte, Eds., Nova University Press, 255–258.

——, and R. W. Houghton, 1987: Atlantic seasonality: I Observations. *Further Progress in Equatorial Oceanography. A Report of the U.S. TOGA Workshop on the Dynamics of the Equatorial Oceans, Honolulu HI, August 11–15, 1986,* E. J. Katz and J. M. Witte, Eds., Nova University Press, 215–233.

Carton, J. A., and B. Huang, 1994: Warm events in the Tropical Atlantic. *J. Phys. Oceanogr.* **24,** 888–903.

Chao, Y., and S. G. H. Philander, 1993: On the structure of the southern oscillation. *J. Climate,* **6,** 450–469.

Hastenrath, S., and L. Heller, 1977: Dynamics of climatic hazards in northeast Brazil. *Quart. J. Roy. Meteor. Soc.,* **103,** 77–92.

Hellerman S., and M. Rosenstein, 1983: Normal monthly wind stress over the world ocean with error estimates. *J. Phys. Oceanogr.,* **13,** 1093–1104.

Hirst, A. C., and S. Hastenrath, 1983: Atmosphere–ocean mechanisms of climate anomalies in the Angola–tropical Atlantic sector. *J. Phys. Oceanogr.,* **13,** 1146–1157.

Horel, J. D., V. E. Kousky, and M. T. Kagaro, 1986: Atmospheric conditions in the tropical Atlantic during 1983 and 1984. *Nature,* **322,** 243–245.

Houghton, R. W., and Y. Tourre, 1992: Characteristics of low-frequency sea surface temperature fluctuations in the tropical Atlantic. *J. Climate,* **5,** 765–771.

Huang, B., 1992: Numerical simulation of the seasonal and interannual variability of the tropical Atlantic Ocean circulation during the 1980s. Ph. D. dissertation, University of Maryland, College Park, 209 pp.

——, and J. Shukla, 1995: A comparison of two surface wind stress analyses over the tropical Atlantic during 1980–87, *J. Climate,* submitted.

Katz, E. J., 1993: An interannual study of the Atlantic North Equatorial Current. *J. Phys. Oceanogr.* **23,** 116–123.

Kutzbach, J. E., 1967: Empirical eigenvectors of sea level pressure, surface temperature and precipitating complexes over North America. *J. Appl. Meteor.,* **6,** 791–802.

Lamb, P. J., 1987a: Large-scale tropical Atlantic surface circulation patterns associated with sub-Saharan weather anomalies. *Tellus,* **30,** 240–251.

——, 1978b: Case studies of tropical Atlantic surface circulation pattern recent sub-Sahara weather anomalies, 1967–1968. *Mon. Wea. Rev.,* **106,** 482-491.

——, P. J., R. A. Peppler, and S. Hastenrath, 1986: Interannual variability in the tropical Atlantic. *Nature,* **322,** 238–239.

Lanzante, J. R., 1984: A rotated eigenanalysis of the correlation between 700-mb heights and sea surface temperatures in the Pacific and Atlantic. *Mon. Wea. Rev.,* **112,** 2270–2280.

Levitus, S., 1982. *Climatological Atlas of the World Ocean.* NOAA Prof. Paper, No. 13, U.S. Govt. Printing Office, 183 pp.

——, 1984: Annual cycle of temperature and heat storage in the world ocean. *J. Phys. Oceanogr.,* **14,** 727–746.

Lough, J. M., 1986: Tropical Atlantic sea surface temperature and rainfall variations in sub-Saharan Africa. *Mon. Wea. Rev.,* **114,** 561–570.

Markham, C. G., and D. R. Mclain, 1977: Sea surface temperature related to rain in Ceara, northeastern Brazil. *Nature,* **265,** 320–323.

Moore, D. W., P. Hisard, J. P. McCreary, J. Merle, J. J. O'Brien, J. Picaut, J.-M. Verstrate, and C. Wunsch, 1978: Equatorial adjustment in the eastern Atlantic. *Geophys. Res. Lett.,* **5,** 637–640.

Moura, A. D., and J. Shukla, 1981: On the dynamics of the droughts in northeast Brazil: Observations, theory, and numerical experiments with a general circulation model. *J. Atmos. Sci.,* **38,** 2653–2675.

Nobre, P. 1993: On the genesis of anomalous SST and rainfall patterns over the tropical Atlantic Basin. Ph.D. dissertation, University of Maryland, College Park, 151 pp.

——, and J. Shukla, 1995: Variations of sea surface temperature, wind stress, and rainfall over the tropical Atlantic and South America, *J. Climate,* submitted.

North, G. R., T. L. Bell, R. F. Cahalan, and F. J. Moeng, 1982: Sampling errors in the estimation of empirical orthogonal functions. *Mon. Wea. Rev.,* **110,** 699–706.

O'Brien, J. J., D. Adamec, and D. W. Moore, 1978: A simple model of upwelling in the Gulf of Guinea. *Geophys. Res. Lett.,* **5,** 641–644.

Pacanowski, R. C., and S. G. H. Philander, 1981: Parameterization of vertical mixing in numerical models of tropical oceans. *J. Phys. Oceanogr.,* **11,** 1443–1451.

Philander, S. G. H., 1986: Unusual conditions in the tropical Atlantic Ocean in 1984. *Nature,* **332,** 236–238.

——, and R. C. Pacanowski, 1986a: A model of the seasonal cycle in the tropical Atlantic Ocean. *J. Geophys. Res.,* **91**(C12), 14 192–14 206.

——, and ——, 1986b: The mass and heat budget in a model of the tropical Atlantic Ocean. *J. Geophys. Res.,* **91**(C12), 14 212–14 220.

——, and W. J. Hurlin, 1988: The heat budget of the tropical Pacific Ocean in a simulation of the 1982–83 El Niño. *J. Phys. Oceanogr.,* **18,** 926–931.

Prohaska, J., 1976: A technique for analyzing the linear relationships between two meteorological fields. *Mon. Wea. Rev.,* **104,** 1345–1353.

Richardson, P. L., and J. K. Mckee, 1984: Average seasonal variation of the Atlantic North Equatorial Countercurrent from ship drift data. *J. Phys. Oceanogr.,* **14,** 1226–1238.

——, and S. G. H. Philander, 1987: The seasonal variations of surface currents in the tropical Atlantic Ocean: A comparison of ship drift data with results from a general circulation model. *J. Geophys. Res.,* **92**(C1), 715–724.

Schopf P. S., and M. J. Suarez, 1988: Vacillations in a coupled ocean–atmosphere model. *J. Atmos. Sci.,* **45,** 549–566.

Servain, J., 1991: Simple climatic indices for the tropical Atlantic Ocean and some applications. *J. Geophys. Res.,* **96**(C8), 15 137–15 146.

——, and D. M. Legler, 1986: Empirical orthogonal function analysis of tropical Atlantic sea surface temperature and wind stress: 1964–1979. *J. Geophys. Res.,* **91,** 14 181–14 191.

——, and J. Merle, 1993: Interannual climate variations over the tropical Atlantic Ocean. *Prediction of Interannual Climate Variations,* NATO ASI Series, J. Shukla, Ed., 153–172.

——, J. Picaut, and J. Merle, 1982: Evidence of remote forcing in the equatorial Atlantic ocean. *J. Phys. Oceanogr.,* **12,** 457–463.

——, M. Seva, S. Lukas, and G. Rougier, 1987. Climatic atlas of the tropical Atlantic wind stress and sea surface temperature: 1980–1984. *Ocean–Air Interact.,* **1,** 109–182.

Suarez, M. J., and P. S. Schopf, 1988: A delayed action oscillator for ENSO. *J. Atmos. Sci.,* **45,** 3283–3287.

Trenberth, K. E., W. G. Large, and J. G. Olson, 1990: The mean annual cycle in global ocean wind stress. *J. Phys. Oceanogr.,* **20,** 1742–1760.

Wallace, J. M., C. Smith, and C. S. Bretheton, 1992: Singular value decomposition of winter sea surface temperature and 500-mb height anomalies. *J. Climate,* **5,** 561–576.

Weare, B. C., 1977: Empirical orthogonal analysis of Atlantic Ocean surface temperatures. *Quart. J. Roy. Meteor. Soc.,* **103,** 467–478.

——, and J. S. Nasstrom, 1982: Examples of extended empirical orthogonal function analysis. *Mon. Wea. Rev.,* **110,** 481–485.

Weisberg, R. H., and T. Y. Tang, 1987: Further studies on the response of the equatorial thermocline in the Atlantic Ocean. *J. Geophys. Res.,* **92,** 3709–3727.

Zebiak, S. E., 1989: Ocean heat content variability and El Niño cycles. *J. Phys. Oceangr.,* **19,** 475–485.

——, 1993: Air–sea interaction in the equatorial Atlantic region. *J. Climate,* **8,** 1567–1586.

——, and M. A. Cane, 1987: A model El Niño–Southern Oscillation. *Mon. Wea. Rev.,* **115,** 2262–2278.